# From toad to frog, a CT-based reconsideration of Bufo servatus, an Eocene anuran mummy from Quercy (France)

Alfred Lemierre, Anne-Lise Folie, Salvador Bailon, Ninon Robin, Michel Laurin

# FROM TOAD TO FROG: DESCRIPTION AND REATTRIBUTION OF THE MUMMIFIED HOLOTYPE OF *BUFO SERVATUS*, AN EOCENE ANURAN FROM FRANCE, BASED ON MICRO-CT EXAMINATION

ALFRED LEMIERRE,[1,*] ANNELISE FOLIE,[2] SALVADOR BAILON,[3] NINON ROBIN,[4] and MICHEL LAURIN[1]

1. CR2P- Centre de recherche en Paléontologie-CNRS/MNHN/Sorbonnes Université, Bâtiment de Géologie, 43 rue Buffon, Paris, 75005, France, alfred.lemierre@edu.mnhn.fr, michel.laurin@mnhn.fr
2. Scientific Survey of Heritage, Royal Belgian Institute of Natural Sciences, 29 rue Vautier, 1000 Brussels, Belgium, afolie@naturalscience.be
3. Département Homme & Environnement, Muséum national d'Histoire naturelle, UMR 7194 HNHP and UMR 7209 AASPE, MNHN-CNRS, 43 rue Buffon, Paris, 75005, France, salvador.bailon@mnhn.fr
4. School of Biological, Earth and Environmental Sciences-University College Cork, Distillery Fields, North Mall, Cork, T23 N73K, Ireland, ninonrobin23@gmail.com

*Corresponding author

# ABSTRACT

In the XIXth century, natural mummies of amphibians were discovered in the Quercy Phosphorites. The specific collection site has never been formally reported, which hampered precisely dating these specimens. The name *Bufo servatus* was erected for one these mummies, based on the external morphology of the specimen.

The tomography of similarly preserved specimens, originating from this same unknown site, revealed almost complete preserved skeletons, preserved soft-tissues and gut contents. We analyze here the holotype of *Bufo servatus* using CT-scanning in order to investigate its potentially preserved internal features. As for the previous specimen, a subcomplete articulated skeleton was identified. Surprisingly, this skeleton is almost identical to that of *Thaumastosaurus gezei*, an Eocene anuran from Western Europe, to which other specimens from this mummy series were previously assigned. Few differences between the specimen skeletons highlight ontogenetic and intraspecific variations, making *T. gezei* a junior synonym of *B. servatus*, creating the new combination *Thaumastosaurus servatus*. Given its association with previously described Quercy specimens, this redescribed anuran is probably from the same time interval as *T. gezei*.

Previous phylogenetic analyses have assigned *T. servatus* to Ranoides, with natatanuran affinities. Using data from this newly described specimen, we test here further its taxonomic affinities. Our analyses confirm this position, and formally identify *T. servatus* as a Natatanuran member of Pyxicephalidae (currently endemic of Equatorial Africa) and more precisely, a stem-Pyxicephalinae. This result confirms the origin of *Thaumastosaurus*, a member of the African herpetofauna occupying Western Europe before the Grande Coupure at the Eocene/Oligocene transition.

# INTRODUCTION

The Quercy Phosphorites consist of a large number of fossil deposits corresponding to large limestones fissures of the Quercy plateau (southwestern France) infilled with clayey phosphates (Fig. 1A-B; Pélissié and Sigé, 2006). During the XIX$^{th}$ century, these fillings were exploited for their use in fertilizer. This operation started in the 1871, with a rapid boom in the number of quarries until 1886, followed a rapid decline, resulting in the closure of almost all quarries by 1893 (Thevenin, 1903; Gèze, 1949). These sites are also well known for their highly diverse vertebrate faunas (see e.g. Filhol, 1877), spanning from Early Eocene to Early Miocene (Sigé et al., 1991; Legendre et al., 1992). Most Quercy phosphorites localities are dated to Middle-Late Eocene to the Late Oligocene, and the associated faunas are of great value to document the impacts of the climatic changes at the Eocene-Oligocene transition (around 33.9 Ma), also named "Grande Coupure" for its extinction feature (Stehlin, 1909). Fossils in the Quercy phosphorites mostly correspond to disarticulated skeletons, representing a highly diverse mammal fauna (Pélissié and Sigé, 2006), as well as a great density of amphibians (Rage, 2006). Beside these assemblage type, a dozen of very differently preserved fossils was collected and reported in the late 1800s (Filhol, 1873). These specimens correspond to exceptionally preserved casts of amphibians (anurans and a urodele) and snakes, in which phosphates have permineralized the tissues of these animals in 3D (Laloy et al. 2013; Tissier et al. 2016, 2017). For these absolutely unique fossil features, these fossils have been referred over centuries to natural mummies (see e.g. Filhol, 1877 for a brief description of the anuran skin) even thoug only the preservation in 3D of their external soft-tissues was then known. They were originally given or sold to the professor Henri Filhol by A. Lafont (or Lafon), pharmacist in Villeneuve (Aveyron, France; see Fig. 1C) during the early 1870s (the first mention is found in Filhol, 1873). They were a part of the private collection of H. Filhol, which housed numerous fossils from the Quercy, including the

holotypes of the taxa he erected. After his sudden death in 1903, Edmond J. de Rothschild bought the entire collection to prevent its dispersal and donated it to the MNHN the same year. Given their unique and striking aspect, they were placed in the paleontological gallery of the Museum, where they remain exposed to the public to this day.

For long, these specimens were thought to be strictly external casts representing the outer aspect of the animals, filled with phosphate sediments (Filhol, 1873). Accordingly, and because of technological limitations, early studies were restricted to their external morphology, and on this basis, they were assigned to different species (*Rana plicata*, *Bufo servatus*; Filhol, 1876, 1877). In the 2010s, two amphibians of these exceptionally preserved series of animals (an anuran and an urodele) were further analyzed using lab-based (on the anuran QU17279; Laloy et al., 2013) and synchrotron light micro-computed tomography (on the urodele QU17755; Tissier et al., 2016, 2017). Both studies evidenced internal subcomplete and articulated skeletons, soft-tissues (e.g. organs) and diet contents, allowing for their complete redescriptions and assessment of phylogenetic affinities (Laloy et al., 2013; Tissier et al., 2016). The anuran taxon turned out to be the most complete specimen of the Eocene *Thaumastosaurus gezei* Rage and Roček, 2007, previously known only from a subcomplete skull and more fragmentary remains (Rage and Roček, 2007). Another member of the mummy series was at the same time assigned to *T. gezei*, based on external shape and some a few visible dermal bones (Rage, 2016).

Here we focus on the last anuran specimen of this series of Quercy exceptionally preserved specimens, left unstudied since the end of the XIX$^{th}$ century: QU17381 (discovered in the 1870s) and originally described as the holotype of new species *Bufo servatus* Fihol 1877. The family assignment of this taxon to Bufonidae was questioned by multiple authors (e.g. Sanchiz, 1998; Rage, 2016) as its identification was based only on its external aspect. As for other Quercy exceptional preserved specimens, tomography revealed a subcomplete

skeleton, as well as several soft tissues, enabling us to reassess the identification of this specimen. The description of the skeleton allows us to make a formal taxonomic attribution for QU17381, and to discuss the name *B. servatus*. Several phylogenetic analyses are performed on this taxon, to discuss its familial attribution. Finally, we discuss the paleobiogeographical impacts caused by the phylogenetic placement of QU17381 and its impact on the fossil record of its clade.

## GEOLOGICAL CONTEXT

**Locality—**QU17381, like the other Quercy "mummies" (Filhol, 1877), is part of the Quercy fossil 'old collection' (MNHN) for which the original location and issuing stratigraphic assignment have never been reported. However, given the brief descriptions given by Filhol (Filhol,1873,1876, 1877), all mummies seem to come from a single quarry.

We believe that the locality that produced the mummies may be either of the two localities discussed below.

The first locality is the town of Villeneuve (Fig. 1), where the first seller (A. Lafont) lived. The hypothesis that this locality produced the mummies is supported by the mention in the description of Filhol (1873) that the series came from the department of Aveyron. This information was also repeated in the local newspapers. At least two of them, the Journal of the Aveyron and the Journal of Villefranche published a small article in January 1874 (shortly after a talk by Filhol at the 'Académie des Sciences de Paris in November 1873) about this discovery and placed it also in Aveyron. However, they are identical, as the writers seem to just have reproduced the text from the talk made by Filhol (Filhol, 1873). In addition, Filhol mentioned in his talk that he had just received the fossils. It is possible that he indicated the Aveyron as the origin of the mummies because the seller came from this place.

Near Villeneuve, around ten quarries are known (Fig. 1C, gray rectangles). Of those ten quarries, one (Vielase) can be ruled out due to the nature of the phosphatic matrix, a tectonized karstic breccia (Simon-Coicon and Astruc, 1991; Legendre et al., 1992), clearly incompatible with the observed thin-scale phosphate replacement of the animal structures. Two other quarries, Cantragrel and les Bories, have yielded fossils and could be compatible, but they are unfortunately inaccessible and their exact location is now unknown. However, they are were dated to the Middle Eocene. The remaining quarries are either azoic, or devoid of any phosphatic matrix still in place for comparison (T. Pélissié, pers. com).

The second locality is the village of Escamps, in the Lot. This department was first mentioned in a local newspaper, the Journal du Lot, also in January 1874, in which an article discussed the future talk by H. Filhol at the 'Société des Sciences Physiques et Naturelle de Toulouse'. Filhol planned to present some exquisitely preserved fossil of anurans that came from a quarry in the Lot. In the Bulletin of the Society, there is an account of this talk, which mentions that there were three anuran fossils (Jeanbernat, 1874). These three exquisitely preserved fossils from the Quercy can only be the mummy series. This reference in the newspaper is not taken from the actual talk, as the article dated from January the 13$^{th}$, 1874 and the talk was given on February 6$^{th}$, indicating that this information probably came from Filhol himself. The fact that the reported locality changed between Filhol's talks in Paris and southern France (Toulouse) could be because he received new information from the seller, which he did not have when first receiving the mummies and giving the talk at the Academy of Sciences (Paris). He probably corrected himself afterwards when receiving more precise information. In addition to this mention in the press and a local learned society, there is a local memory of a discovery of "stone" anuran in the village of Escamps, dating back to the late XIXth century (T. Pélissié and E. Cassan pers. com. october, 2020). A young miner, Emile Dutheil (who was fourteen in 1873) discovered a stony anuran (which corresponds to the

description of a mummy) inside a cavity in a quarry near the town, either in the site ‘les Rosières’ or ‘les Tempories’ (Fig. 1C). This fossil was soon exchanged against a bottle of wine and might have ended in the hands of A. Lafont. What happened after is known (see earlier). The other mummies might have been discovered shortly thereafter. Six sites are regrouped under the name ‘les Rosières’ (Fig. 1C) and are dated from Late Eocene MP17a (37.8 to 37.4 Ma) to MP19 (34.5 to 33.5 Ma; Aguilar et al., 1997; Vandenberghe et al., 2012). They have been partially studied in the previous decades (Remy et al., 1987), without any discovery of a new mummy, but the series discovered in the XIX$^{th}$ century could have come from a small pocket within one of these six sites. The other site, ‘les Tempories’ is dated from the MP19 (Late Eocene, 34.5-33.5 Ma). In situ layers of phosphorites are still visible today (T. Pélissié pers. com) but most of the site was drained during its exploitation and later used as a landfill. If the series came from a precise layer within the quarry, this layer may have been completely cleared out more than a century ago.

A last hypothesis is that the series came from elsewhere in the Lot. As a matter of fact, the various fossils discovered in the quarries were often collectibles for the local notables, and exchanges or sales were not uncommon between the notables of each town and village. Some of these fossils were then sold to known museum curators, or even donated in exchange for favors (T. Pélissié pers. com.). This hypothesis is almost impossible to refute, unless a precise account of the discovery, with information on the location, is found.

The evidence about each locality reviewed above does not unambiguously identify the source of the mummies. However, the strongest support is for the locality of Escamps, especially because of the local memory of such a discovery, which does not occur in the vicinity of Villeneuve. We thus putatively identify the locality as the village of Escamps, Lot (France), giving a Late Eocene age for the mummy series.

**Stratigraphic range—**The genus *Thaumastosaurus* (to which two of the mummies have been attributed so far) is known from various localities in Western Europe (Vasilyan, 2018). The earliest remains of *Thaumastosaurus* are from the MP16 (Late Middle Eocene ~39.5 Ma) from two Swiss localities, and the genus is present throughout the Late Eocene, with most of the localities located in the Quercy phosphorites. The geologically most recent record of *Thaumastosaurus* is from the MP20 (~33.5 Ma) from Escamps, in France. The complete list of the localities where *Thaumastosaurus* is identified was compiled by Vasilyan (2018: table S1).

A recent study (Ősi et al., 2019) presented disarticulated bones from the Upper Turonian (Early Upper Cretaceous) and attributed a fragmentary maxilla to *Thaumastosaurus* (Ősi et al., 2019: fig. 6A-E) and a vertebra to an Anura indet. They supported their tentative attribution of the vertebra to *Thaumastosaurus* based on a ventral keel also putatively present in *T. gezei* (Ősi et al., 2019: fig. 6F–G; Laloy et al., 2013: fig. 5C). However, what Ősi et al. (2019) interpreted as a ventral keel on the vertebrae illustrated in Laloy et al. (2013) is in fact the ridge of the neural spine, visible by transparency. In addition, in the vertebral column of QU17381, there is no ventral keel on the vertebrae (see below). Furthermore, given the fragmentary state of this vertebra, this cannot be attributed to a smaller clade than Batrachia (Duellman and Trueb, 1994; Tissier et al., 2016). The ornamentation composed of irregular pits and ridges, found on the maxilla described by Ősi et al. (2019), occurs in numerous Cretaceous anuran clades (Roček and Nessov, 1993; Roček, 2008; Company and Szentesi, 2012; Báez and Gómez, 2018) as well as more recent anurans and other taxa (e.g. squamates, crocodilians, various early stegocephalians; Buffrénil et al., 2015) and is not diagnostic of *Thaumastosaurus*. Moreover, the oval foramen located near the processus pterygoideus (if the fragmentary element is indeed a maxilla) is present in other anurans (Biton et al., 2016). This

makes the attribution of these Upper Cretaceous fragments to an Eocene anuran taxon very unlikely. They could belong to a wide range of anurans clades present during the Mesozoic.

We therefore here conclude that *Thaumastosaurus* has a stratigraphical range from the Late Middle Eocene (~39.5 Ma) to the Terminal Late Eocene (~33.5 Ma).

## MATERIALS AND METHODS

**Institutional abbreviations—IC2MP:** Institut de Chimie des Milieux et Matériaux de Poitiers, Poitiers, France *;* **MHNT.PAL**: Muséum d'Histoire Naturelle de Toulouse, Toulouse, France ; **MNHN**: Muséum National d'Histoire Naturelle, Paris, France ; **NHMB**: Naturhistorisches Museum Basel, Basel, Switzerland ; **UM:** Université de Montpellier, France.

The mummy MNHN QU17381, currently displayed in the paleontology gallery of the National Natural History Museum in Paris (France), was scanned at the PLATINA (PLATeforme INstrumentale d'Analyses) platform at the IC2MP (Poitiers, France). A microfocus beam of 160 kV of the CT-scanner was used with the following parameters: voltage, 130 kV current, 180 µA; voxel size, 0.024 µm; slice resolution, 1346 × 2525 pixels. A total of 1750 virtual slices showing internal structures were reconstructed using XAct (RX solution) These slices were imported in the 3D reconstruction software Mimics 21.0 (Materialise, Leuven, Belgium). Before the importation, the slices were cropped to remove a maximum of empty spaces. To decrease the data size, the slices were converted from 16 bits to 8 bits, dividing the data size by two. The dataset thus includes 1256 slices with a resolution of 1527 x 2391 pixels and a voxel of 2.4 µm. The 3D model was produced by segmentation of each bone using the 'thresholding' function (using the contrast on greyscale images). We used the same voxel resolution of 2.4 µm, with a smoothing factor of 3 for one iteration, to

homogenize the model resulting from manual segmentation. Data produced by segmentation were exported in the software 3matic 9.0 for PDF 3-D creation (available in Supplementary Information).

Tomography revealed the internal preservation of soft tissues replicated in calcium phosphate (e.g. part of the brain and of the spinal cord, potential muscles and nerves). Unfortunately, most of the soft internal structures are either too degraded, or too similar to other structures in density and/or capacity to absorb X-rays (resulting in poor contrast) to be correctly segmented and described here. The external structures will be described in detail in Robin et al. (in prep) and are only briefly presented here. Our description focuses on the skeleton. The skull preserved inside the mummy is missing its anteriormost region (the snout) but is otherwise complete. Some hyobranchial bones are preserved, along with most of the postcranial bones, except the limbs and pelvic girdle. An isolated ilium (PRR 2002) collected in 1984 (Rage, 1984a) was recently attributed to *Thaumastosaurus* (Vasilyan, 2018). As the postcranial of the two species of *Thaumastosaurus* described in the Quercy, *T. gezei* Rage & Roček, 2007 and *T; botti* De Stefano, 1903, is very similar (Vasilyan, 2018), we used this specimen for the scoring of *T. servatus* in the dataset for phylogenetic analysis.

The anatomical terminology used herein is based on Roček (1980) and Biton et al. (2016) for cranial features, Sanchiz (1998) for postcranial ones, and Gómez and Turazzini (2016) for iliac characters.

**Phylogenetic analyses—**In total, our matrix includes 86 taxa and 143 morphological characters (62 cranial and 68 postcranial ones, 12 of the hyobranchial apparatus, and one from soft-tissues), taken form Báez and Gómez (2018; see Appendix 1–3 for the list of characters). We added 15 new extant natatanuran taxa, leading to a better representation of the major

natatanuran clades inferred from recent molecular phylogenies (Frost et al., 2006; Pyron and Wiens, 2011; Jetz and Pyron, 2018). The data for those new taxa were recovered from literature (Procter, 1919; Clarke, 1981; Scott, 2005; Evans et al., 2014) and from 3D-model made available on Morphosource by the Blackburn Laboratory (Florida, USA) as part of the OVert program (Cross, 2017; for more information see the website: https://www.floridamuseum.ufl.edu/overt/).

All analyses were performed using TNT v 1.5 (Goloboff and Catalano, 2016). They were performed using equal weighting for half of them, and implying weighting with various values of the concavity constant (k) for the other half, some with all characters unordered and others with cline characters ordered (characters 3, 9, 10, 14, 26, 34, 51, 52, 68, 93, 112, 121, 124, 125 and 126), with or without topological constraints. All analyses consisted of heuristic searches with 1000 random addition sequences of taxa, followed by tree bisection reconnection (TBR) branch swapping, holding 10 trees per repetitions. The final trees were rooted on *Ascaphus truei* (Ascaphidae) and, when more than one tree was obtained, a strict consensus was processed.

Implied weighting was used to minimize the influence of homoplastic characters in the dataset, and achieved a better resolution of the different uncertainties recovered in the analysis under equal weighting (Goloboff, 1993, 1997), mostly for morphological characters (Goloboff et al., 2018a) and several values of k were used (k = 1–20) to assess sensitivity of the results due to variations of the strength of the function (Goloboff et al., 2008). Some controversies remain on the effectiveness of this method, especially when compared to Bayesian models (O'Reilly et al., 2016; Congreve and Lamsdell, 2016; Puttick et al., 2017), but some authors recently presented evidence that implied weighting performs well (Goloboff et al., 2018a, b). Consequently, we chose using both equal and implied weighting parsimony methods to compare their results. Cline characters were ordered, as recent studies (Rineau et al., 2015,

2018) have shown that analyses using ordered morphocline characters outperformed analyses using unordered characters even if the ordering scheme includes some errors (Rineau et al., 2018). Constrained analyses were performed with ordered characters including both equal and implied weights (k = 7), using the topology of Jetz and Pyron (2018) as a constraint for extant taxa. The same was done using the topology presented in Feng et al. (2017), with extinct taxa as floating taxa, in both cases. Node supports were expressed using Bremer support and standard bootstrap, with traditional searches of 1 000 replicates, collapsing groups below 5%. Bremer support uses tree fit score (Bremer, 1994; Goloboff and Farris, 2001). However, in implied weighting analyses, Bremer is expressed in fractions due to the different weighting that actually reflect the character fit (Goloboff, 1997). The resulting Bremer support is thus expressed in fractions (Jones and Butler, 2018).

## SYSTEMATICS PALEONTOLOGY

**Anura** Duméril, 1805

**Neobatrachia** Reig, 1958

**Ranoides** Frost et al., 2006

**Natatanura** Frost et al., 2006

**Pyxicephaloidea** Bonaparte, 1850

**Pyxicephalidae** Bonaparte, 1850

***Pyxicephalinae*** Bonaparte, 1850

Genus ***Thaumastosaurus*** De Stefano, 1903

*Enigmatosaurus* Nopcsa, 1908

Type species: ***Thaumastosaurus bottii*** De Stefano, 1903

**Revised Diagnosis—**Hyperossified natatanuran exhibiting cranial extosis (sensu Trueb, 1973), resulting in an ornamentation, composed of pits and ridges, on the frontoparietals, maxillae, nasals, squamosals and sphenethmoid; nasals and frontoparietals co-ossified with each over and with the sphenethmoid and prooticooccipital (frontoparietals only), rhomboid dorsal fenestra on the skull allowing for a dorsal exposure of the sphenethmoid; palatines (neopalatines of Trueb, 1973) present, in medial contact with each over (by their margo medialis); anterior tip of the processus cultriformis of the parasphenoid does not extend between palatines; processus posterolateralis and ramus paroticus of squamosals merged, articulating with the crista parotica of the otic capsules; arteria occipitalis enclosed in a canal on the frontoparietals; medial ramus of the pterygoids well-developed, overlapping the parasphenoid alae; zygomatic ramus (lamella alaris + processus maxillaris) of the squamosals well-developed, articulating (longer than its otic ramus) with the maxillae.

Differs from *Pyxicephalus* Tschudi, 1838 and *Aubria* Boulanger, 1917, in lacking fang-like lamellar projection on the dentaries, in having the alary process of the premaxillae oriented dorsally (instead of posterodorsally), the articulation for the lower jaw at the same level as the occiput instead of posterior to it and the clavicles oriented anteromedially (instead of perpendicularly),

Differs further from *Pyxicephalus* in having the alae of the parasphenoid perpendicular to its processus cultriform (instead of posterior to it), a dorsal exposure for the sphenethmoid, cotyles of the atlas fully confluent (Type III of Lynch, 1971) instead of juxtaposed (Type II), bicuspid teeth on the maxillae and in lacking a lateral wall of the neurocranium ossified around the optic foramen.

Differs from *Aubria* in having keels on the ventral surface of the parasphenoid, a distinct postchoanalis processus of the vomers and a high pars facialis of the maxillae on all its length.

***Thaumastosaurus servatus*** Filhol, 1877 nov. comb.

*Rana plicata* Filhol, 1876: 27. Holotype specimen figure 401, 4012, 404, 405 of Filhol (1877), MNHN QU17279.

*Bufo serratus* Filhol 1876: 28. Gymnonym (Nomen nudum). Holotype, specimen figure 412 (413 in error) of Filhol (1877), MNHN 17381.

*Bufo servatus* Filhol, 1877: 493. Holotype, specimen figure 412 (413 in error) of Filhol (1877), MNHN 17381.

*Thaumastosaurus gezei* Rage & Roček, 2007. Holotype MNHN QU 17376; fig. 1, 7A.

*Rana cadurcorum* Martín et al., 2012: 163. Alloneonym. Holotype same as replaced name *Rana plicata* Filhol, 1877.

**Holotype—**MNHN QU17376, articulated skull missing anterior end, right side of palate, much of the right cheek region, parts of parasphenoid and both otic capsules (Rage and Roček, 2007: fig. 1, 7A). Unrecorded locality on the Quercy Phosphorites, southwestern France. Age uncertain, but probably late Middle to Late Eocene.

**Referred Specimens—**MNHN QU17748, right squamosal missing anterior tip of lamella alaris (Rage and Roček, 2007: fig. 2); MNHN QU17279, nearly complete specimen lacking the appendages and pelvic region (Laloy et al., 2013: fig. 1A–C); MNHN QU17280, forelimb (Laloy et al., 2013: fig. 1D, E); MNHN unnumbered, specimen preserving the head and part of the trunk; MNHN QU17381, nearly complete specimen lacking the snout, appendages and pelvic region.

**Revised Diagnosis—** Differs from *T. wardi* by having a longer anterior extension of the squamosal alongside the dorsal margin of the maxilla, forming the whole lateral margin of the orbit, a lamina horizontalis of the maxilla circular (convex) rather than flat in medial view and in having the ridge separating the fossa maxillaris from the posterior part of the maxillae oriented posteriorly (instead of anteriorly).

Differs from *T. bottii* by having an elongate and slender medial process of the premaxillae, no ventral longitudinal ridge on this same process, and a groove for the vena jugularis interna shallower and wider.

## DESCRIPTION

**External Preservation—**As part of the Quercy old collection mummies, QU17381 displays an exceptional three-dimensional preservation including most of its external soft-tissues replicated in calcium phosphate. These include the two eyeballs (Fig. 2A) and the skin laying over 3D-preserved muscular series (Fig. 2B–F), the striations of which are locally visible ventrally (eg. right submaxillary muscles) (Fig. 2F). The specimen corresponds to a 6 cm-long subcomplete body, extending from the snout, almost fully preserved on its right part, to the sacrum. Hindlimbs and forelimbs seem to be only proximally present. Posteriorly to the eyeball, a 1.3x0.6 cm large ovoid swelling is present (Fig. 2D, represented by a "?"). This was at first identified as the outer visible deformation of a parotoid gland, typical of bufonids anurans (Duellman and Trueb, 1994). However, subsequent authors doubt the presence of these parotoid glands on QU17381 (Piveteau, 1927; Rage, 2006). The 3D model of the specimen shows that this swelling is caused by the processus posterior of the squamosals, which goes slightly out of the body and stretches the skin in this area (Fig. 3). This structure might have been caused by desiccation (Robin & al, in prep).

QU17381 outer tissues are non-homogeneously preserved. The skin shows a higher level of pristine preservation on the ventral and lateral sides of the specimen with neat sub-millimetric foldings. The latter concentrate on the mandible/maxillary complex, as well as posterior to the eye (Fig. 2B–D). These folds, absent on extant anurans when alive, must result from post-mortem deformation of the outer tissues. Dorsally, the replicated surface tissues reveal a glassy aspect reflecting a different phosphatized texture (Fig. 2C, E). In this region, the skin and inner tissues do not retain their in vivo volume but appear to be collapsed over the spine and underlying bony structure. The desiccation (or differential chemical transformation) of this dorsal part of the integument during early decay may have occasioned laterally the wrinkling of the skin resulting in observed microfolds. The left eyeball shows at the bottom a neat demarcation of eye with surrounding skin membrane (Fig. 2C). Elsewhere, no distinction between the eye and the eyelid can be seen.

Two other anuran specimens of the Quercy phosphates display this level of exceptional 3D preservation in calcium phosphate. MNHN QU17279 shows neat eyelids covering the eyes fossilized in their original direction (Fig. 4A, C). On this specimen, the skin, more outstretched, is preserved homogeneously over the specimen surface revealing thinner skin microfolds and a local bulbous texture which looks original to the structure (Fig. 4A–C). Larger skin ridges exptend posteriorly from the eyes (Fig. 4B). About 1 mm in width, they correspond to original dorsolateral folds present in many anuran taxa (Duellman and Trueb, 1994), especially in ranoids (e.g. in Pyxicephalidae, see Poynton, 1964; Channing and Baptista, 2013; Channing et al., 2016; see Dubois and Ohler, 2005 for other ranoids). On the right lateral side of the specimen, in a region between the processus posterior and the postero-lateral side of the squamosal, the skin bears a slight demarcation, with a faint outline (Fig. 4C). Given the preservation of the skin on this region (Fig. 4A–C), this delimitation is not the

results of the bones underneath. In extant anurans, this region houses the tympanic membrane (Duelleman and Trueb, 1994).

The second best-preserved specimen, MNHN QU17376, which consist solely of a head, shows a gradual variation in outer tissue preservation from snout to neck (Fig. 4D–E), with snout bony ornamentation (part of the nasals) emerging (Fig. 4D). Posterolaterally, the skin looks pristine, with bulbous textural components. On these external aspects, the specimen QU17381 (Fig. 2) may plausibly have undergone a longer decay/exposure time before burial than QU17279 (Fig; 4A–C) and comparable or shorter than QU17376 (Fig. 4D–E).

**Skull**

The skull is incomplete, missing the anteriormost part and the premaxillae (Fig. 2, 3, 5).). The preserved cranial bones are all articulated.

**Dermal Bones—**The frontoparietals, squamosals, maxillae, nasals and the exposed rhomboid area of the sphenethmoid bear dermal ornamentation composed of deep oval to subcircular pits and ridges with a constant thickness (Fig. 5A). The dermal sculpture on the sphenethmoid is much less marked than on the other bones and restricted to exposed dorsal area.

**Frontoparietals—**The frontoparietals are fused into a single bone, in the shape of a truncated rhomboid, longer than wide, without any clear trace of the median suture between them. However, anteriorly, at the posterior end of a deep notch on the midline of the margo nasalis, a shallow depression on the dorsal and ventral face seems to mark the limit between the bones (Fig. 6A). Anterolaterally, they are connected to the nasals by the external margin of the margo nasalis, and medially, with the posteromedial margin of the dorsal exposure of

the sphenethmoid. The margo lateralis bears on its mid-length an external expansion (a peak), the tectum supraorbtialis (Fig. 6A–B). There is no contact between frontoparietals and squamosals (Fig. 5A), but the lateral expansion of the tectum may indicate the existence of a ligament between these bones, delimiting the posterior margin of the orbit, as observed in some extant anuran (Roček, 1980).

Posteriorly, the frontoparietals are fused to the prooticooccipital complex (Fig. 5D). The processus lateralis of the frontoparietals are difficult to distinguish from the crista parotica of the prootic but seem to form an almost straight margin (Fig. 5A, 6A). Posterolaterally the processus paraoccipitalis of the frontoparietals are also fused to the dorsal face of the prominentia ducti semicircularis posterioris of the prootic, forming a prominent ridge (Fig. 5D). The processus paraoccipitalis also delimits medially the foramen for the arteria occipitalis canal (Fig. 5D). As in several extinct and recent anurans (Sanchiz, 1998) the processus posterior of the frontoparietals consist of a horizontal lamina, extending midlength of the posterior margin of the bone and forming a small spike-like surface covering the dorsal exposure of the prooticooccipital (Fig. 6A).

Anterolaterally, the pars contacta consist of a vertical lamina extending from the ventral surface of the frontoparietals (Fig. 5B) and is fused to the dorsolateral part of the sphenethmoid (Fig. 5B, 6A). It increases in size posteriorly, forming a thin vertical lamina that is fused to the prootic and to the processus lateralis, covering anterolaterally the prootic (Fig. 5B).

Ventrally, the incrassatio frontoparietalis presents two structures, the facies cerebralis anterior, and the facies cerebralis posterior (Fig. 6B). The facies cerebralis anterior is an unpaired lanceolate structure, extending from the posterior margin of the sphenethmoid/frontoparietals suture. The posterior limit of this structure is not clear. The facies cerebralis posterior is an unpaired circular impression, located postero-laterally on the

left side of the bone. In the other mummy (QU17381), a similar condition was found, and a facies cerebralis posterior is present on each side (Laloy et al., 2013: fig. 4D). This condition is reminiscent of ranoids (Jarošová and Roček, 1982). In our specimen, the unpaired condition might be due to a non-preservation of the impression, or a lesser ossification of the right frontoparietal.

**Squamosals—**In lateral view, the lamella alaris is arch-shaped and anteriorly narrow; it expands anteriorly before dwindling in the vicinity of the processus maxillaris (Fig. 6C), forming a thin strip of bone separating the maxilla from the orbit (Fig. 5B). This configuration is similar to the one of QU1727, which also bears an elongate thin extension of the lamella alaris (Laloy et al., 2013) but is shorter than the one of the holotype of *Thaumastosaurus gezei* (MNHN QU 17376; Rage and Roček, 2007). The anterior end of the lamella alaris forms a shallow groove with the lateral end of the nasal, identified as the nasolacrimal duct (Fig. 5B).

The processus maxillaris is antero-posteriorly elongated (Fig. 6C). The processus zygomatico-maxillaris of the maxilla is inserted into an incisura lateral to this processus maxillaris, fully overlapping it. This is not visible in lateral view, as it is overlapped by the lamella alaris (Fig. 5B). The margo orbitalis is concave dorsally, forming the lateral wall of the orbit (Fig. 5A–B). Laterally, the lamella alaris extends posteroventrally into a spike-like extension, reaching the anterior part of the processus posterolateralis.

Medially, the ramus paroticus is a broad dorsoventrally flat lamina, fused to the crista parotica of the otic capsule dorsoventrally (Fig. 5A). It narrows medially and ends in an almost straight margin (Fig. 5A). The processus posterior of the squamosal is short and rounded distally (Fig. 5A–B, 6B). The processus posterolateralis is elongate and slender. In dorsal view, the surface between the ramus paroticus and the processus posterolateralis is concave (Fig. 5A), and most likely forms the lateral wall of the tympanic cavity (Roček and Lamaud, 1995). The processus posterolateralis bears a medial flange fused to the ramus posterior of the pterygoid, making the

proper segmentation of both separated parts difficult (Fig. 5B–C) and its distal end is fused to the dorsal surface of the processus glenoidalis of the quadratojugal (Fig. 5B).

**Maxillae—**The maxillae are not fully complete; the left one stops at the processus frontalis level and lacks the anterior part of the bone, the right maxilla is almost complete, missing the most anterior part of the bone. Posteriorly, the processus posterior, long, with a low height, is in contact with the quadratojugal (Fig. 5B), the contacting area forming a groove in medial view (Fig. 6D). The processus pterygoideus, visible in medial view, is short and marked by a small posterior prominence from the lamina horizontalis. The lamina horizontalis is straight and with a moderately thickened medial border, anteriorly, it extends dorsally up to the lamina anterior. This processus delimits ventro-medially a large pit, which faces posteriorly. The lamina horizontalis is straight and with a moderately thickened medial border, anteriorly, it extends dorsally up to the lamina anterior. Posterior to the processus pterygoideus, the lamina horizontalis narrows considerably, ending in a thin, poorly marked strip delimiting the lower margin of the processus posterior of the maxillae (Fig. 6D). In medial view, the lamina horizontalis is pronounced and developed into an anterodorsal anterior spine (Fig. 6D), marking the base of the lamina anterior.

In lateral view, a flattened smooth processus zygomatico-maxillaris (posterior), as well as a well-developed processus frontalis (anterior) are visible dorsally (Fig. 6E). The dorsal margin of the pars facialis, is almost straight. A weakly-pronounced notch is visible on the midline of this margin (Fig. 6E). This notch was also observed in non-articulated maxillae in *Thaumastosaurus* (Roček and Lamaud, 1995; Vasilyan, 2018). On the medial surface of the maxilla, the lamina horizontalis broadens, and a groove for the palatoquadrate bar is present dorsally to the lamina (Fig. 6D). The recessus vaginiformis is overlapped by a medial crista extending up to the tip of the processus frontalis. Anteriorly, the fossa maxillaris is shallow (Fig. 6D).

The ventral margin of the lamina horizontalis delimits the base of the crista dentalis up to a triangular anterior facet of the maxillae in medial view (articulation of the premaxilla; Roček and Lamaud, 1995: fig. 6D). The teeth are present, but they are difficult to discern on either maxilla, it is not possible to determine if they are uni- or bicuspid, and whether or not they were pedicellate. However, Holman and Harrison (2002) described a partial maxilla attributed to *Thaumastosaurus*, where the teeth are pedicellate and bicuspid. The pedicellate condition was also retrieved in another partial maxilla (Holman and Harrison, 2003). The tooth row ends anterior to the posterior margin of the lamina horizontalis.

The anteriormost portion of the maxillae, bearing the end of the lamina anterior, the rostellum and the anterior extension of the crista dentalis, is not preserved.

**Nasals—**The nasals are in close contact anteromedially (Fig. 5A). This puts them in a transitionary state between the condition found in the first mummy (QU17381; Laloy et al., 2013), in which they are separated by an empty space, and the condition of the holotype of *T. gezei*, where they are wholly fused, with no trace of a midline suture (Rage and Roček, 2007). They diverge posteromedially, leaving the sphenethmoid exposed. They are fused to the dorsal surface of the sphenethmoid. The margo maxillaris and margo orbitalis are concave, with the processus paraorbitalis forming a tip oriented posterolaterally, like the processus posterior (Fig. 5A, 6F). The processus paraorbitalis is devoid of any dermal ornamentation distally. This smooth surface is delimited ventrally by the anterior extension of the lamella alaris of the squamosal, forming a groove for the nasolacrimal duct (Fig. 5B, 6F). The processus parachoanalis is a small protuberance, located at midlength of the margo maxillaris (Fig. 6F).

The nasals are attached to the frontoparietals between their processus posterior, leaving an opening in the dorsal face of the dermal skull, with the sphenethmoid exposed (Fig. 5A). The dermal sculpture appeared to be more deeply pitted near the margo orbitalis.

## Suspensory Bones

**Quadratojugals—**As in all other anurans, the jugals and quadrates are fused when ossified (Duellman and Trueb, 1994), forming the quadratojugals (Fig. 7A). They are elongate, with an anterior slender and elongate processus jugularis and a posterior thick protuberance, the processus glenoidalis. The quadratojugals articulate with the maxillae on a long triangular facet, located on the lateral side of the processus jugularis, on nearly one half of its length (Fig. 5B, 7A). In dorsal view, the processus jugularis is a slender long curved lamina that extends up to 80% of the pterygoid fossa. The processus glenoidalis, is relatively small compared to its proximal part. It can be divided in the midline by a deep groove, which is overlapped by the processus posterolateralis of the squamosal (Fig. 5B). Medially, the processus glenoidalis is overlapped with the distal part of the ramus posterior of the pterygoid. Neither lateral nor dorsal process can be observed on either bone.

**Angulosplenials—**Both angulosplenials are incomplete. The left angulosplenial represents less than ¼ of the whole bone (compared to the one described in Laloy et al., 2013), and the right one represents around 2/3 of a complete angulosplenial. The Mentomeckelian bones and dentaries are missing as well. The processus coronoideus is well developed, forming an oval (dorsoventrally oriented) flattened plate, with the crista paracoronoidea being poorly developed, almost non-observable (Fig. 7B). The crista mandibulae externa is marked laterally, on the opposite side of the processus coronoideus. The sulcus cartilagine Meckeli (pro cartilago in Roček, 1980) on the lateral side of the angulosplenial, widening posterodorsally (extremitas spatulata, Fig. 7B). The articulation of the lower jaw is preserved, with the posterior end of the angulosplenials connected to the processus glenoidalis of the quadratojugal, forming a flare on the dorsal surface of the bone.

## Palate Bones

**Palatines—**The palatines (neopalatines of Trueb, 1973) are an elongate, flattened dorsoventrally bony sub-cylindrical elements, perpendicular to the maxilla. In ventral view, both palatines are in contact with each other by their margo medialis, in the midline of the sphenethmoid, as in QU17376 (Rage and Roček, 2007). The processus palatines maxillae extends posteriorly (posterolaterally) on the palatoquadrate groove of the maxilla (Fig. 5C, 7C). The medial processus ventrally contact the lateral process of the sphenethmoid is almost in contact posteriorly with the anterior tip of the parasphenoid.

**Vomers—**Both vomers are present, still in place, articulated to the ventral face of the sphenethmoid and to themselves by their lamina medialis, forming a flat lamina that extends posteromedially (Fig. 5C). The margo medialis is round and is almost in contact with the palatine. The left vomer is damaged and at least half of it is missing, but a few teeth are visible in ventral view (Fig. 5C). Vomerine teeth were not visible on the right vomer during the segmentation, but their presence is observed by Laloy et al. (2013) in their segmentation of QU17279. The processus anterior extends anterolaterally towards the anterior spine of the lamina horizontalis of the maxilla, but without contacting it. The processus choanalis anterior is very elongate and extends laterally without reaching the maxilla. The processus choanalis posterior is a small flattened lamina, with a crest extending dorsally (Fig. 7D). The margo choanalis (in Roček, 1994) is well-marked, at an acute angle indicating a moderately large choanal opening (Biton et al., 2016).

**Parasphenoid—**The parasphenoid is posterolaterally fused to the prooticoocipital complex and anteriorly to the sphenethmoid. The anterior tip of the processus cultriformis is almost in contact to the medial tip of the palatines (Fig. 5C). The processus cultriformis is long and slender, without any longitudinal ridges on its surface. Posteriorly, the alae (processus lateralis) are perpendicular to the processus cultriformis, shorter than this and bear a transversal and arched keel on their ventral surface (Fig. 7E). The posterior margin is

anteriorly concave towards a short, medially borne spear-like processus posterior. The parasphenoid is fused to the pterygoids by the anterolateral margin of the alae. This suture was very hard to represents during the segmentation, but the alae appear to be fairly overlapped by the ramus interior of the pterygoid anteriorly (Fig. 5C).

**Pterygoids—**The pterygoids are of the standard triradiate shape (very common among anurans, Fig. 5A). The ramus posterior is composed on an elongated vertical lamina (partly fused to the processus posterolateralis of the squamosal) in contact distally with the processus glenoidalis of the quadratojugals (Fig. 5C). The ramus interior bears a posterodorsal flange that forms a part of the posterior wall of the orbit (Fig. 5D).

A deep sulcus extends dorsally from the ramus posterior to the ramus anterior on the margo maxillaris, called the sulcus pterygoidus (Fig. 7F). The ramus anterior is well-developed, robust, and slightly flattened dorsoventrally.

**Endocranium**

**Sphenethmoid—**The sphenethmoid is a pentagonal and unpaired bone. Most of its dorsal surface is overlapped by the nasals and frontoparietals and fused to these bones, leaving only a small rhomboid exposed surface (Fig. 5A). This exposure is covered with low and poorly defined ornamentation composed of pits and ridges, nearly identical to the one covering the dermal bones (Fig. 5A, 8A). A difference in the size of the ornamentation is a marker for the ontogeny in extant anurans (Buffrénil et al., 2015, 2016), as the dermal ornamentation of the sphenethmoid (and other bones as well) grows thicker with the growth. This difference was also observed, with an even weaker ornamentation, in one other specimen, (QU17381; Laloy et al., 2013), indicating that our specimen was probably more adult than the other mummy.

The posterior chamber, housing the forebrain and its olfactory bulbs (Scalia, 1976). Anteriorly, the bone is divided into two chambers (cavitas nasalis) separated medially by the septum nasi (Fig. 8C). These anterior chambers form the posteromedial walls of the nasal capsules, that connect to the forebrain by the olfactory nerves (Duellman and Trueb, 1994). The bone is elongate posteriorly, reaching around half the length of the parasphenoid (Fig. 5C). Despite the global hyperossification of the skull, the sphenethmoid does not reach the prooticooccipital, leaving a part of the lateral walls of the braincase unossified, probably cartilaginous.

Posteriorly, the dorsal fenestra frontoparietalis forms a notch, allowing the space for the insertion of the facies cerebralis anterior (Fig. 8A) of the frontoparietals, bearing a dorsal impression of the forebrain. Ventrally, the sphenethmoid is fused to the anterior tip of the parasphenoid and to the palatines. The processes lateralis are distally short, with the posterior wall slightly more extended laterally (Fig. 8A). The dorsal surface of these processes extends slightly postero-laterally, forming a poorly developed lamina supraorbitalis (Fig. 8A). The lateral wall of each anterior chamber is pierced by a foramen, the canalis ramus medialis nervi ophthalmici (passage for the ophtalmic nerve), opening into a large cavitas nasalis (= anterior chamber) (Fig. 8B).

Several portions of the anterior sections of the sphenethmoid are partially ossified, which is characteristic of hyperossification. The septum nasi is ossified, without any anterior thickening, reaching the anterior part of the nasals (Fig. 8C), and the tectum nasi is oriented anterodorsally, forming a triangular flattened area in dorsal view (Fig. 8A). The solum nasi (ventral surface of the cavitas nasalis) bears a thickening on its surface, the sella amplificans, forming a broad prominence raised dorsally (Fig. 8C). The surface of those structures (solum nasi, septum nasi) appears smooth in the segmentation. This most likely indicate that a cartilaginous part was present (Roček and Lamaud, 1995; Duellman and Trueb, 1994). The

rest of the anterior part of the sphenethmoid was most likely cartilaginous or very poorly ossified, and so the postnasal wall and anterior wall of the nasal capsule were not preserved.

In ventral view, the sphenethmoid is subcruciform, with the lateral expansion of the anterior chamber perpendicular to the posterior chamber and the bony anterior extension of the septum nasi.

**Prooticooccipital complex—**The prootic, occipital and exoccipital are fully fused, without any visible suture, and form the posterior part of the braincase and skull (Fig. 5D). The otic capsule are poorly ossified ventrally, producing an irregular surface (Fig. 8G).

The foramen magnum is large and slightly compressed dorsoventrally, forming an oval opening. The two condyles occipitalis are crescentic, with a small ridge dorsally connecting them to the prominentia ducti semicircularis posterioris (Fig. 8D). These latter are compressed laterally, arising into an elongate protuberance oriented ventrolaterally. Medially, they delimit a dorsoventral depression, which is delimited dorsally by a small median keel (Fig. 8D). This keel is similar to the one found in QU17376 (Rage and Roček, 2007: fig. 5B) and NHMB V.R31 (Vasilyan, 2018: fig. 3) but is not visible in QU17279 (Laloy et al., 2013).

Two large foramina, the foramen jugularis, are partially hidden in posterior view by the condyles occipitalis (Fig. 8D). They open in the lateral wall of the cavum cranii and in the otic capsule. The fenestra ovalis are located on the lateral wall of the prootic (Fig. 8D). They are large foramina, closed ventrally by the parasphenoid, and mark the main entrance to the otic capsule (Fig. 5C–D).

Dorsally, the crista parotica extends laterally into a dorsoventrally compressed processus (ramus lateralis sensu Špinar, 1978) (Fig. 8D–E). On its distalmost margin, two foramina are visible, opening into the ramus paroticus and the processus posterolateralis (both of squamosal), into the anterior and lateral wall of the tympanic cavity. Just ventral to the

crista parotica, a cavity houses the stapes, with a foramen, the foramen tympanum. A groove (groove in Fig. 8D) extends from the foramen jugularis and this foramen is visible on the posterior surface of the otic capsule and might have housed a perilymphatic canal. This groove is visible in both specimen QU17279 and QU17376 (Rage and Roček, 2007; Laloy et al., 2013).

Dorsally, the parietal fenestra is large, with the tectum synoticum poorly developed, extending into a triangular anterior lamina (Fig. 8E–F). However, this large opening is covered by the frontoparietals, leaving no exposure of the underlaying fenestra in dorsal view. This region housed the cerebellum, connected to the otic capsules.

Anteriorly, the foramen prooticum is large, not subdivided (unlike in QU17376; see Rage and Roček, 2007: fig. 7). The groove for the vena jugularis is shallow and not well delimited (Fig. 8F), as in QU17279 and QU17376 (Rage and Roček, 2007: fig. 7A). However, this groove is more visible than in QU17279, being nearly identical to the one found in QU17376. No other foramen is visible in this groove, except for a notch on the left prootic that could resemble the second foramen found in QU17376 (Rage and Roček, 2007), but without any bone covering the lateral part of this foramen. This might be linked to ontogeny, as this foramen is not known in the youngest *Thaumastosaurus* specimen (Laloy et al., 2013). Medial to the anterior surface of the prominentia ducti semicircularis posterioris, a small depression is present, also known in QU17279 (Fig. 8E). It might be another part of the otic canals.

The lateral wall of the cavum cranii is pierced by numerous foramens. As mentioned earlier, the posteriormost is the opening leading to the foramen jugularis. Another large irregular opening is present, leading to the otic capsules. It allowed the passage for the ganglion and central nerve VIII, from the medulla oblongata (housed near the cerebellum) and the otic capsule (Duellman and Trueb, 1994). This irregular shape might be the result of a poor preservation, resulting into the fusion of the two foramina leading from the brain to the otic

capsule. A small rounded foramen is also located on this wall and could be a perilymphatic foramen.

**Stapes—**Both stapes are preserved. The footplate is compressed at midlength, forming a bifurcation and is also slightly compressed in medial view, forming a notch posteroventrally. The processus medialis plectri extends up to the squamosal in a long slender rod (Fig. 8H), slightly curved ventrally.

The fenestra ovalis of the exoccipital is wider than the footplate, implying the presence of an operculum located in front of it, unfortunately not preserved. This is reinforced by the posteroventral position of the notch on the footplate, which is used as the anterior border where the upper rim of the operculum is inserted (Bolt and Lombard, 1985). Both stapes are at the same position on each side of the prooticoocipital, so they should still be in anatomical position.

On the various mummies of *T. gezei*, a tympanic membrane can be observed (Fig. 4C), but no tympanic annulus was preserved. In the clade to which *Thaumastosaurus* belongs (see Phylogeny), all taxa still possess a complete tympanic annulus, but it has been lost in several anuran clades, the best-known being the Bufonidae (Pereyra et al., 2016). However, the presence of this membrane implies the presence a tympanic annulus (Pereyra et al., 2016). It would have been housed in the tympanic cavity formed laterally by the ramus paroticus, the processus posterior and the processus posterolateralis of the squamosal (Fig. 5B–D). The distal extension of the ossified processus medialis plectri, ending near this region, could indicate a rather short cartilaginous part (the processus externa plectri) near the contact between stapes and tympanic annulus.

**Hyobranchial Skeleton**

**Hyoid bones—**The cartilaginous hyoid plate is not preserved, or not visible on the scan. However, two slender bony elements, the thyrohyal bones, corresponding to the posteromedial process of hyoid plate are present. The two elements are oriented anteromedially, their proximal part almost in contact. They widen at both tips (proximal and distal) (Fig. 8I). They are placed ventrally under the first three vertebrae and the exoccipital, and dorsal to the coracoids and clavicle.

## Postcranial Skeleton

### Vertebral Column

The vertebral column is similar to the one found and described inside the mummy by Laloy et al. (2013). It is composed of eight presacral vertebrae, one sacral vertebra and an urostyle (Fig. 9).

**Atlas—**The atlas is articulated to the exoccipital by 2 elongate and large cotyles (Fig. 10A), confluent, meeting in a protruding lip at the midline, forming a large articular facet with the skull (type III of Lynch, 1971). The neural canal is large, with thin lateral walls and thicker ventral and dorsal walls, the latter forming a large base for the neural spine which is short and inclined posteriorly (Fig. 9B). The postzygapophyses are poorly developed, with a flattened articular surface inclined medioventrally. The centrum is flattened dorsoventrally and possesses a small oval shaped condyle (Fig. 10B).

**Post-atlantal vertebrae—**The centrum of the post-atlantal vertebrae are longer than wider and compressed dorso-ventrally (Fig. 9B–C). The centrum of vertebrae II–VII is concave anteriorly and convex posteriorly, indicating a procoelous condition.

In lateral view, the neural arch is thin, anteriorly notched, with an enlarged base (Fig. 9B). Arches are non-imbricated. The neural canal remains broad until the fifth post-atlantal vertebra. The neural spines are dorsally tall and inclined posteriorly, but no more than the

posterior margin of the postzygapophysis. The posteriormost post-atlantal vertebrae (vertebra VI to VIII) possess a shorter neural spine, which are oriented less posteriorly. The zygapophyses have flat articular processes. No vertebra bears ribs. These latter are replaced by the transverse processes of the vertebrae.

The first post-atlantal vertebra (Vertebra II) possesses distally large transverse processes, a bit shorter than the sacral apophyses (transverse process in Fig. 10C–D). They are slightly posteriorly arched (Fig. 9A, C). The processes are thicker at their mid-length, with a crest appearing on the anterior face. The second post-atlantal vertebra (Vertebra III) possess the largest transverse processes, larger than the sacral apophyses. They are oriented lateroventrally and moderately widen distally. The transverse processes of vertebra IV have the same distal extension as the sacral apophyses and are oriented lateroposteriorly. The presacral vertebrae V–VII are similar, possessing transverse processes thinner and narrower distally. On vertebra V they are slightly oriented posterodorsally (Fig. 9B). On vertebrae VI and VII, they are perpendicular to the axial column axis. Presacral vertebra VIII bears thin transverse processes similar to the one of the previous presacral vertebrae. However, this vertebra is amphicoelous.

**Sacral Vertebra—**The sacral vertebra possesses two small well separated (medially) posterior, circular condyles that articulate with the urostyle, and one dorsoventrally flattened oval anterior condyle that articulates with the posterior cotyle of the last presacral vertebra (Fig. 10C–D). On the anterodorsal border of the neural arch, a high and well-developed dorsal lamina is present, extending from the base of the apophyses to the base of the neural spine (Fig. 9A, 10C). The dorsal margin of the neural canal bears a well-marked lamina anteriorly and posteriorly (Fig. 10C-D). The sacral transverse processes are subcylindrical in cross section, slightly flattened dorsoventrally, and almost do not widen distally. A small notch is

visible dorsally on the distal margin of both transverse processes (Fig. 9A) and probably served as an insertion for the ilia. The neural spine is reduced and anterodorsally oriented.

**Urostyle—**The urostyle is posteriorly incomplete. The anterior portion of the bone is articulated with the sacral vertebra with two well-separated circular anterior cotyles (fossa cotylae), which emerge laterally from the main shaft of the urostyle (Fig. 10E). The neural canal is moderately wide, accounting for half the height of the neural arch. The neural arch bears a well-developed thick dorsal process. This also marks the cranial end of a tall and thin carina dorsalis that extends throughout the whole preserved portion of the bone and slightly decreases in size posteriorly (Fig. 10F). A spinal foramen is present on each base of the carina dorsalis, just posteriorly to the thick dorsal process (Fig. 10F). No transverse processes are present.

**Pectoral Girdle**

All pectoral bony elements are present in anatomical position (Fig. 11).

**Scapulae—**The scapulae are clearly dorsoventrally elongate, with a moderately widened distal end of the processus anterior. The margo anterior is concave, and the margo dorsalis bears a groove on its entire length, which represents the suprascapular articulation (Fig. 12A). There is no crest on both anterior or posterior margines Ventrally, the processus acromialis and the processus glenoidalis are separated by a moderately wide sinus interglenoidalis (Fig. 12B), The processus acromialis is wider than the processus glenoidalis and rounded at its distal (ventral) margin; in lateral view, it hides the processus glenoidalis and the sinus interglenoidalis. In medial view, a well-developed medial crest is present on the processus glenoidalis, extending on its entire length, up to the base of the processus anterior, (Fig. 12A). No anterior lamina is present on the processus anterior. The glenoid fossa is moderately extended dorsoventrally (Fig. 12A).

**Coracoids—**The coracoids are oriented lateromedially, with the processus glenoidalis thickened and circular in cross section. The processus glenoidalis of both coracoids and scapulae are almost in contact with each other, leaving a gap where the paraglenoid cartilage was located. The processus epicoracoidalis is flat and anteroposteriorlly enlarged (much larger than the processus glenoidalis) and bears a rounded distal margin (Fig. 12C). It extends anteriorly, forming a hook, which ends close to the clavicles distal end. Both coracoids are in contact with each other medially, but do not overlap (Fig. 11). This is characteristics of a firmisternal condition (sensu Cope, 1864; Boulanger, 1886). The left coracoid is badly damaged, with the processus glenoidalis broken off from the main shaft (Fig. 12D–E). On the anterior and posterior margins of the main shaft, vertical laminae can be observed, forming a bony callus linking the two broken parts. This callus is also visible in ventral view, expanding the width of the shaft of the coracoid (Fig. 12D–E). This damage can be linked to the missing part of the left clavicle. The absence of almost any disarticulated bones (except the ilia) and the presence of a mineralized skin on this part of the specimen seems to exclude the diagenesis hypothesis. The absence of any hole indicating a missing part in the area of the coracoid and clavicle (the nearest holes are located anteriorly on the ventral face of the specimen) excludes the extraction hypothesis. This leaves only the hypothesis of a damage received before the burial of the animal. In extant anurans, the healing process for fracture are the same as in mammals, but with a slowest ossification process (Cameron et al., 2012; Egawa et al., 2014). Given that the broken coracoid seems partially fused back and bears a bony callus, this may represent a scar from a wound received during the life of the animal.

**Cleithra—**The cleithra are partially ossified, forming a broad bony plate dorsal to the scapulae. The margo vertebralis is almost straight (slightly rounded), and the ramus anterior is long and slender, slightly curved posteriorly (Fig. 12F). There is no ramus posterior, so the cleithra are not bifurcated. The margo anterior expands medially, forming a lamina (lamina

recurvata sensu Špinar, 1972) extending on its entire length (Fig. 12G). The cleithra are broad ventrally, with a rounded margo posterior and margo scapularis (Fig. 12G).

**Clavicles—**Both clavicles are preserved, but only the right one is complete, the left one being represented only by its proximal part (Fig. 11). This could be linked to the injury visible on the left coracoid. The clavicles are almost as long as the coracoids, slightly arched anteriorly, and anteromedially oriented. In dorsal view, the proximal part is bifurcated and articulates with the processus acromialis and processus glenoidalis of the scapulae, forming a part of the fossa articularis for the humeri. The sulcus cartilagine praecoracoidealis extends posteriorly on the length of the bone (Fig. 12H). The clavicles are in contact, slightly overlapping dorsoventrally the processus glenoidalis of the coracoids. The extremitas medialis of the clavicle is not in contact with the distal part of the coracoids (Fig. 11).

**Sternum—**The sternum is fully ossified, consisting of an elongate slender element, which widens distally, the anterior end being the largest (Fig. 12I). It is strongly similar to the one found in *Pyxicephalus adspersus* (Sheil, 1999: fig. 5B).

**Omosternum—**The omosternum is ossified, denoting a firmisternal condition of the girdle (Cope, 1864; Boulanger, 1886; Duellman and Trueb, 1994). It exhibits a bifurcated posterior end (Fig. 12J).

**Forelimb**

**Humeri—**The proximal parts of both humeri are preserved, although badly damaged. The right humerus is preserved with only its articular facet with the glenoid fossa of the pectoral girdle. The left humerus however, is better preserved, with its articular facet with the glenoid fossa of the pectoral girdle and a part of the diaphysis (Fig. 13A). Considering the size of other partial humeri associated to *Thaumastosaurus* (see Laloy et al., 2013; Rage, 2016), this may represent a third of the complete bone. The left humerus shows the presence

of a moderately developed crista ventralis, and the absence of a proximal crista paraventralis (Fig. 13A).

**Pelvic Girdle**

**Ilia—**The two ilia are partially preserved. The left one is only a fragment of the distal part (around 1.4 mm), but the right one is better preserved. It represents maybe half or more of the ilial shaft (= processus cylindriformis). It bears a high and well-developed dorsal crest (Fig. 13B). Unfortunately, the rest of the ilium (distal half) is not preserved, as in the first mummy (Laloy et al., 2013).

## TAXONOMY

QU17381 is the holotype of *Bufo servatus*, a species erected by H. Filhol (1877) based on a single specimen described a few years earlier (Filhol, 1873) and illustrated in the monograph (Filhol, 1877: pl. 51; fig. 412). There are some inconsistencies between description (Filhol, 1873), where it is indicated that the left part of the head is missing, and the figures, where the specimen appears complete (Filhol, 1877). However, Filhol also named the same specimen *Bufo serratus* earlier (Filhol, 1876). This nomen is not available as Filhol (1876) does not give characters to diagnose the taxon, only those allowing generic allocation. Martín et al. (2012) considered the nomen *B. servatus* available but did not discuss the criteria for availability. Filhol justified his attribution of *B. servatus* to the Bufonidae by the presence of parotoid glands, as well as other characters that allowed to differentiate this taxon from other *Bufo*, unfortunately not specified (Filhol, 1877; Piveteau, 1927), thus failing to provide a diagnosis. Nevertheless, an illustration of the specimen on which the name is based was published by Filhol (1877: fig. 412).

According to the article 12.2.7 of the International Code of Zoological Nomenclature (ICZN), a figure can be considered as an indication for a nomen if published before 1931, so the name *B. servatus* is available. This name has been cited several times since its original description (Piveteau, 1927; Tihen, 1962; Sanchiz, 1998; Rage, 2006) and its validity was not often discussed. Sanchiz (1998) considered the name a nomen vanum (Mones, 1989), a taxonomic term considered in the ICZN as referring to a name based on a type inadequate for definitive diagnosis, without questioning its validity.

The attribution to the genus *Bufo* was based on the presence of what he identified as two parotid glands located right behind the eyes. However, several studies (Piveteau, 1927; Tihen, 1962; Rage, 2006, 2016) have since considered this observation to be erroneous. We suggest that the structures interpreted by Filhol as parotoid glands are artefactual skin ridges caused by the desiccation of the body after the death during the natural mummification process. In addition, on specimen QU17381, we observed teeth on the maxillary, which are lost in the Bufonidae (Duelleman and Trueb, 1994). Moreover, the vertebral column is diplasiocoelous, which is characteristic of the Ranoidea. Finally, the presence of a firmsternal pectoral girdle, as well as an ossified osmosternum, also reinforce the attribution to a ranoid taxon. We consider that QU17381 cannot be attributed to Bufonidae or *Bufo*. Furthermore, the skeleton of specimen QU1738 is almost identical to the one of QU17279 and to the skull of QU17376, both attributed to the genus *Thaumastosaurus*. We therefore attribute the specimen QU1738 to *Thaumastosaurus* De Stefano, 1903 by the following combination of characters: (1) dermal bones covered with ornamentation that differs from the one found in *Latonia*, *Pelobates*, *Eopelobates* and *Ceratophrys*; (2) nasals (partially) and frontoparietals co-ossified with each other and with sphenethmoid and frontoparietals co-ossified with prooticooccipital; (3) rhomboid part of sphenethmoid exposed on skull roof; (4) no contact between the frontoparietal and squamosal; (5) palatines present, in medial contact with each other; (6)

anterior tip of the parasphenoid does not extend between palatines; (7) processus posterolateralis and ramus paroticus of squamosal merged, articulating with the crista parotica of the otic capsules (Rage and Roček, 2007; Vasilyan, 2018).

At the specific level, QU17381 differs from *Thaumastosaurus bottii* and *T. wardi* by the anterior extension of the lamella alaris of the squamosal which makes up the entire lateral margin of the orbit on QU17381 whereas it ends at midlength on *T. bottii* and *T. wardi*. However, the squamosal described with the neotype of *T. bottii* (Roček and Lamaud, 1995: fig. 5) bears a lamella alaris almost entirely broken off, and the length of its anterior extension cannot be asset. Other squamosals attributed to *T. bottii* also seems broken, or with the anterior part of the bone eroded (Vasilyan, 2018: fig. 4G–H), making this difference dubious. Given that isolated squamosals attributed to *T. gezei* also present a broken anterior extension of the lamella alaris (Rage and Roček, 2007: fig. 2), this difference might only be the result of a different preservation, as we are still lacking an articulated skull of *T. bottii* as complete as the holotype of *T. gezei*. Although the full extension of the lamella alaris is not attained in a younger stage (see QU17279 in Laloy et al., 2013), the absence of any anterior extension is not known in *T. gezei* (Laloy et al., 2013). This difference is not attributed to ontogeny.

The specimen QU17381 furthermore differs from *T. bottii* by having on the prooticooccipital complex, a shallow, poorly delimited groove for the vena jugularis interna (Fig. 8F), whereas *T. bottii* possesses a narrower, and more sharply delimited groove (Roček et Lamaud, 1995; Vasilyan, 2018). Other characters have been proposed to distinguish the two Quercy species, but they are all located on the premaxilla (Vasilyan, 2018), which is missing in QU173981.

Among the mummies attributed to *Thaumastosaurus*, QU173981 presents strong resemblances with QU17279, the former holotype of "*Rana plicata*" (attributed to *Thaumastosaurus gezei* by Laloy et al., 2013), with the anterior extension of the squamosal

separating the maxillary from the orbit by a thin strip, and a postcranial identical in both mummies. It also bears a strong resemblance to QU17376, with the palatines medially in contact with each other and a groove for vena jugularis interna which also resembles the one of QU17279 (Laloy et al., 2013). However, a few differences can be seen between our skull and those of QU17279 and QU17376. First, the nasals are partially fused, and not separated in the midline as in QU17279, but not as fully fused as in QU17376. Likewise, the sculpture of the sphenethmoid is more marked than in QU17279, but less than in QU17376, where it is identical to the one found in the nasals and frontoparietals, forming an almost continuous dermal ornamentation. As in QU17279, the foramen prooticum is not divided into two portions. However, as mentioned in the description, a notch can be observed on the lateral margin of the anterior surface of this bone in continuity with the groove for the vena jugularis, and could be the first anterior foramen found in QU17376 and other *Thaumastosaurus* sp. skulls (Rage and Roček, 2007:fig.7A–C). The extension of the lamella alaris is also thinner than in QU17376, resembling the one found in QU17279. Those differences can be linked to ontogeny (Laloy et al., 2013).

Specimen QU17381 shares with specimen QU17379, holotype of *T. gezei*, and QU17279, assigned to *T. gezei*, the anterior extension of the squamosal (forming the whole lateral wall of the orbit) and the shape of the groove for the vena jugularis interna which is shallow and wide. Both characters are listed in the diagnosis (see above). The specimen QU17381 can therefore be assigned to *Thaumastosaurus gezei*. This assignment makes the three-known anuran "mummies" from the Quercy Phosphorites attributed to this species.

A consequence of this attribution is that *T. gezei* and *B. servatus* are synonyms. Considering the available names and excluding those invalidated by homonymy, *Bufo servatus* Filhol, 1877 is the oldest available nomen. We therefore here consider that the valid name of this taxon is *Thaumastosaurus servatus* Filhol, 1877 (new combination).

Furthermore, specimen QU17381 can be placed between specimens QU17279 and QU17376 (youngest to oldest) in an ontogenetic series, representing a subadult stage of *Thaumastosaurus*. This indicates that the skull of *Thaumastosaurus* progressively becomes more hyperossified, with the growth of the dermal ornamentation of the sphenethmoid and the growth of the palatines, extending medially.

**Taxonomic review of the *Thaumastosaurus* species**–Four species have been attributed to the genus *Thaumastosaurus*: *T. bottii* Roček and Lamaud, 1995; *T. wardi* Holman and Harrison, 2002, *T. sulcatus* Holman and Harrison, 2003; and *T. servatus* Filhol, 1877. Among them, *T. bottii* and *T. servatus* are found in the Quercy. As said previously, the differences between these two species are based on the skull, as the postcranial of *T. bottii* is scare, and seems identical to the one of *T. servatus* (Vasylian, 2018). The two other species are described from the Eocene of England. Those two species are based on a very few bones, and their diagnoses need to be reassessed.

*Thaumastosaurus wardi* was differentiated from other species of *Thaumastosaurus* by having (1) a lamina horizontalis of the maxilla flat rather than circular in medial view; (2) the ridge separating the fossa maxillaris from the posterior part of the maxillae oriented anteriorly rather than posteriorly; (3) teeth larger and less numerous; (4) a different ornamentation; (5) the orbital margin of the squamosal hemispherical and curved; (6) a rounded rather than straight base of the ramus paroticus. However, the original description of *T. servatus* shows that character (5) has a broader taxonomic distribution, as *T. servatus* also has an orbital margin of the squamosal curved and hemispherical. The ramus paroticus of *T. wardi* is incomplete on the only specimen known and illustrated (Holman and Harrison, 2002: fig. 3, 4) so the character (6) cannot be confirmed (also noted by Vasilyan, 2018). The difference of size and number of teeth (character 3) can be explained by ontogeny, or infraspecific variation (Rose, 1968). The difference in ornamentation has already been shown to reflect ontogeny or

preservation (Rage and Roček, 2007; Vasilyan, 2018) and cannot be taken as a solid evidence to diagnose closely related species. The only characters left to diagnose *T. wardi* are characters (1) and (2), basing this species on its maxillae. Numerous differences have been pointed out between the diagnoses of *T. bottii* and *T. servatus* based on their premaxillae, but this bone is unknown in *T. wardi*.

The second English species is *Thaumastosaurus sulcatus*, diagnosed by having (1) a different ornamentation of the dermal bones; (2) the lamina horizontalis thinner and more sharply bowed upward; (3) a more extensive contact area for the premaxillae; (4) tooth crowns narrow and pointed, with pigmentation (reddish to brown); (5) the dorsal portion of the ramus paroticus of lamella alaris arising more posteriorly; (6) the ventral border of the squamosal less deeply concave (Holman and Harrison, 2003). As indicated previously, the difference of ornamentation cannot be used as solid evidence to differentiate a new species as it typically varies with the ontogeny (Buffrénil et al., 2015; Vasilyan, 2018) and can be altered during diagenesis (Roček and Lamaud, 1995; Rage and Roček, 2007; Vasilyan, 2018). In addition, this pattern was also found in other small and presumably young specimen attributed to *Thaumastosaurus bottii* (Vasilyan, 2018). Furthermore, the tooth characteristics can have different origins, as in *T. wardi*, as well as the diagenetic process of pigmentation. Tooth pigmentation is known in some extant and extinct mammalia extinct mammalia (Dumont et al., 2014; Smith and Codrea, 2015), salamander (Clemen, 1988; Anderson and Miller, 2011) and fish (Suga et al., 1992) and linked to the presence of iron oxides. This pigmentation can be related to a reduction of dental wear (Dumont et al., 2014) or resistance to acid (Kato et al., 1988) or reflect random phylogenetic changes (Suga et al., 1992). However, this is unknown in any extant anuran, and this pigmentation could be an alteration of a mineral in the enamel during the diagenesis. Furthermore, the short extension of the pigmentation (only the crown of the tooth) is strange, as in salamanders, it extends onto the whole teeth (Anderson and Miller,

2011) and its function is unknown. Without any chemical analyses, and the very small number of maxillae available (two fragmentary maxillae bearing teeth), we cannot conclude that this pigmentation is unique to *T. sulcatus*. The characters observed on the squamosal were made on one partial bone (Holman and Harrison, 2003), making their validity dubious (e.g. dorsal portion of the ramus paroticus not fully preserved). The contact area for the premaxillae is of similar size in several maxillae of *T. servatus* and *T. bottii* (Laloy et al., 2013; Vasilyan, 2018). The width of the lamina horizontalis can be linked to ontogeny and is like the one found in *T. servatus* (Rage and Roček, 2007; Laloy et al., 2013). *T. sulcatus* should thus be considered "nomen dubium" unless new materials reveal unique diagnostic characters.

## PHYLOGENY

*T. servatus* was first suggested to have affinities with Leptodactylidae, especially the south American Ceratophryidae, based on cranial characters (Roček and Lamaud, 1995; Rage and Roček, 2007). Later on, Laloy et al. (2013), in the description of the subcomplete skeleton found within a mummy, carried on a phylogenetic analysis which includes *Thaumastosaurus* within Ranoides, using a matrix modified from Báez et al. (2009). This latter dataset (see Báez et al., 2009) was itself based on the matrix proposed by Fabrezi (2006) modified for ceratophryid phylogeny. The dataset from Báez et al. (2009) included 42 taxa, 3 of which were extinct taxa, scored for 75 mostly osteological characters. Laloy et al. (2013) enlarged the sample by adding taxa from Evans et al. (2008), whose matrix was also modified from the dataset of Fabrezi (2006; see Evans et al., 2008 for modifications) and included genera as OTUs. Evans et al. (2008) had delete one character (the dorsal exposure of sphenethmoid) and redefining one (character 1 in Evans et al., 2008; Laloy et al., 2013). Laloy et al. (2013) found

*Thaumastosaurus* within the Natatanuran, as the sister-taxon of a clade that contains *Pyxicephalus* and *Ceratobatrachus*.

In 2018, Báez and Gómez modified the dataset from Báez et al. (2009), adding numerous neobatrachian taxa and redefining characters to test the impact of hyperossification characters within the dataset. The taxa sample was greatly enlarged (from 42 to 71 taxa), and 68 characters were added or redefined. Among the taxa, *T. servatus* was included, using the new information brought by QU17279 described by Laloy et al. (2013). They also found *T. servatus* within hyperossified Natatanuran, but as the sister-taxon of *Pyxicephalus adspersus* Tschudi, 1838 (African bullfrog) instead of *Ceratobatrachus guentheri* Boulanger, 1884 (Solomon island leaf frog). This topology could be explained by the limited inclusion of only five extant natatanurans taxa in their dataset. We therefore expanded the dataset with 15 extant natatanurans taxa (See Materials and Methods for more information). We increased the taxnomic sampling of our matrix in the Pyxicephalidae, represented previously only by *Pyxicephalus adspersus* (the sister-taxon to *T. servatus*, according to Báez and Gómez, 2018), to explore the potential relationships with *T. servatus*, adding seven taxa from the clade. They are *Arthroleptella lightfooti*, *Aubria subgillata*, *Cacosternum boettgeri*, *Cacosternum namaquense*, *Natalobatrachus bonebergi*, *Strongolypus grayii*, *Tomopterna tuberculosa*.

Most extant anurans are placed within the Neobatrachia (Feng & al., 2017). This taxon includes two clades, the Hyloides and the Ranoides. The latter clade can be divided in three parts, the Microhylidae (*Phrynomantis*, *Dermatonotus*, and *Coxicephalus* in our dataset), the Afrobatrachia (*Arthroleptis* and *Phlyctimantis* in our dataset) and the Natatanura (represented by 19 taxa in our matrix, of which 14 were not previously included in any of the other matrices mentioned above), between which the phylogeny remains contentious. Natatanura represents the vast majority of extant Ranoides (Frost et al., 2006; Pyron and Wiens, 2011), but its fossil record is scarce and mostly composed of isolated fragmentary bones (Rage,

1984b; Sanchiz, 1998; Gardner and Rage, 2016). Given the good preservation and completeness of *T. gezei* fossils, understanding its precise position within Natatanura is essential to better understand the evolution of the clade and assess the timing of its diversification. For this, several phylogenetic analyses are performed, as detailed below.

**Unconstrainted analysis**

**Equal Weight analysis, unordered—**We obtained 140 MPTs (most parsimonious trees) of 1355 steps (CI = 0.122; RI = 0.326) with the analysis performed under equal weight, with all multistate characters unordered (Fig. S3A). The strict consensus shows numerous polytomies, with Neobatrachia not recovered. *Thaumastosaurus servatus* is recovered as a sister-taxon to a trichotomy composed of hyperossified ranoides, *Pyxicephalus adspersus*, *Aubria subsigillata* and *Ceratobatrachus guentheri* (Fig. S3A). The clade is supported by 26 synapomorphies. Many of them have been considered to be associated with the Ranoides and Natatanura, which are not recovered in this analysis.

**Equal Weight, ordered analysis—**With cline characters ordered, we obtained 90 MPTs, of 1373 steps (CI = 0,137; RI = 0,422; Fig. 14A, S3B). The strict consensus is more resolved than with unordered states, but it still presents numerous polytomies. A majority of the ranoids taxa (excluding the three microhylids) are clustered together (Fig.14A; Fig. S3B), forming a “Ranoides” clade. This restricted “Ranoides” is supported by nine synapomorphies but has poor bootstrap support (less than 5%) and moderate Bremer support. Among those synapomorphies, the ossification of omosternum (101: 0–>1) is uniquely shared by members of this clade; it is present in almost all taxa forming the “Ranoides” clade, except in *Cacosternum.* Another one, non-overlapping coracoids (104: 0–>1), is convergent with only the Microhylids (see Appendix S in Supplement Data 1 for the detailed list).

The presence of an ossified omosternum is particularly important in several phylogenies of Ranoides and Natatanura, as various authors have proposed it as a synapomorphy for either clade (Lynch, 1973; Laurent, 1986; Scott, 2005; Frost et al., 2006). Most natatanuran taxa display this character, although it is lost in some taxa typically ranked as genera. It is present in the Afrobatrachia but not in the Microhylidae. Another interesting synapomorphy recovered is the presence of non-overlapping epicoracoids, found as a synapomorphy for both the "Ranoides" clade and the Microhylidae clade (present in all extant Ranoides, as mentioned in Trueb, 1973; Lynch,1973; Frost et al., 2006). This character represents a firmsternal condition for the pectoral girdle, classically associated with the Ranoides (Trueb, 1973; Lynch, 1973; Duellman and Trueb, 1994). However, this condition is also found as a synapomorphy for the Dendrobatidae (Trueb, 1973; Frost et al., 2006).

*Thaumastosaurus servatus* is found within the "Ranoides" clade, recovered as a sister-taxon to a trichotomy composed of the extant hyperossified Ranoides (Fig. 14A). Nine synapomorphies were recovered, almost all of them based on cranial elements, and six of which are hyperossification-linked characters, like the presence of a surpraorbital flange on the frontoparietals (6: 0–>1), a contact between squamosals and nasals (11: 0–>1; lost in *Ceratobatrachus guntheri*) and the presence of a heavely ornamented external surface of the pars facialis of the maxillae (50: 0–>2; see Appendix S6 in Supplement Data 1 for the detailed list). The clade seems mainly moderately supported by the convergent evolution of hyperossification characters present on the skull, and is quite similar to the previous analysis, where *T. gezei* was recovered, close to extant hyperossified ranoids (Laloy et al., 2013; Báez and Gómez, 2018).

The two afrobatrachians (*Arthrolepis adolfifriederici* and *Phlyctimantis verrucosus*) are recovered in a clade with *Arariphrynus placidoi* (Fig. 14A), which is poorly supported by the loss of the ossified style of the sternum (102: 1–>0), the reduction of the width of the

glenoid fossa (112: 1–>2; relative to the width of the shaft), the loss of the posterolateral process of the hyoid plate (67: 1–>0) and the reduction of the posterodorsal expansion of the the ischium (131: 1–>0). Of those four synapormophies, only the reduction of the glenoid fossa is scored *A. placidoi*. The latter is recovered as the sister-taxon of *Phlyctimantis*, supported by three synapomorphies, which are the reduction of the length of the urostyle (92: 1–>0), relative to the presacral vertebral length, a pars facialis of the maxillae which decrease abruptly in height in the orbital region (49: 0–>1) and a change in the shape of the occipital condyles, which become stalked (40: 0–>1). In addition, the *A. placidoi* postcranial is not well-known, and the synapomorphies for the "Ranoides" clade recovered (mentioned earlier) are not known in this taxon.

**Implied weighted analysis—**When using implied weighting with a low concavity constant (k = 3), we obtained one fully resolved tree (CI = 0.164; RI = 0.533) (Fig. S4). Neobatrachia was recovered as monophyletic, with *Heleophryne* as a sister-taxon to all others neobatrachian. The neobatrachian clade is poorly supported by six synapomorphies including the presence of palatines (27: 0–>1; see Appendix S6 in Supplement Data 1 for the detailed list). Although not unique to the clade, this synapomorphy is commonly used, along other character coded here but not recovered as synapomorphies for the clade (the loss of free ribs in adults and a bicondylar articulation between the sacral vertebra and the urostyle; Báez et al., 2009) to characterize neobatrachian taxa. Another synapomorphy proposed for this clade, the presence of a taeniae tecti medialis in the frontoparietal (Haas, 2003) was not recovered, likely for the fact that this character was not scored for a majority of the taxa in the dataset.

We recovered a monophyletic "Ranoides" (excluding Microhylidae), still supported by seven synapomorphies, including six found previously. *T. servatus* is placed as a sister-taxon to the crown-clade of Pyxicephalinae (Fig. S4 in Supplement Data 1). This clade is

moderately supported by twelve synapomorphies on cranial and postcranial characters (see Appendix S6 in Supplement Data 1 for the detailed list). One of them, the presence of a contact between squamosals and nasals (11: 0–>1) is interesting as it is considered a marker for hyperossification (Báez and Gómez, 2018; Paluh et al., 2020) and is recovered only in the Pyxicephalinae and the Ceratophryidae.

When using a higher constant value (k = 7), we obtained two MPTs (CI = 0.168; RI = 0.548). In the strict consensus (Fig. 14B; Fig. S5), *T. servatus* is placed within the Pyxicephalinae, as a sister-taxon to *Aubria subsigillata* (brown ball frog). This clade is poorly supported by s single synapomorphy, the absence of odontoids on palatines (reversion to the plesiomorphic state). The Pyxicephalinae is supported by three synapomorphies, the developpement of a contact between nasals and squamosals (11: 0–>1), the ossification of the planum anteorbitale of the sphenethmoid (33: 0–>1) and the development of a process lateral to the anterior process of the hyale (64: 0–>1; unknown in *T. servatus*). Only one of these was found in the previous analysis (contact between nasals and squamosals). As mentioned above, this character is retrieved as a synapomorphy for the Ceratophryidae (Báez and Gómez, 2018). *Ceratobatrachus guentheri* was placed as a sister-taxon to the Pyxicephalinae (including *T. servatus*), supported by ten synapomorphies. Many of these were recovered in the equal weight analysis, and are linked to hyperossification characters like the contact of nasals along most of their medial margin (3: 0–>2), the developpement of superorbital flange on the frontoparietals (6: 0–>1) or the developpement of the ramus paroticus of the squamosals, overlapping prootics (14: 1–>2; see Appendix S6 in Supplement Data 1 for the detailed list)..

When using even higher constant value (k = 12), we retrieved one fully resolved MPT (CI = 0.171, RI = 0.558; Fig. S6). *T. servatus* is recovered in the same position as before, within the Pyxicephalinae, with *C. guentheri* as the closest taxon to all Pyxicephalinae. *A.*

*placidoi* is placed once again within the Afrobatrachia (as when using equal weight), supported by the same synapomorphies.

**Constrained analyses**

Relationships within Ranoides and Natatanura have always been controversial (Clarke, 1981; Lynch, 1973; Scott, 2005 Frost et al., 2006; Pyron and Wiens, 2011), with various clades lacking morphological synapomorphies. This can be observed in our analysis as well, as we did not recover the Ranoides as a clade, but only a subset of these excluding microhylids (see Fig. S3–6).

However, molecular datasets have yielded a better resolution of their relationships, especially with large dataset (Frost et al., 2006; Pyron and Wiens, 2011; Feng et al., 2017; Jetz and Pyron, 2018). Some uncertainties remain, with some clades still lacking clear support (see Pyron and Wiens, 2011). Conflict still exist around the position of the Afrobatrachia, either as a sister-taxon to the Microhylidae (Pyron and Wiens, 2011; Jetz and Pyron, 2018) or to the Natatanura (Feng et al., 2017). We choose to run the dataset constrained under two different topologies, to see if changes in the relationship inside the Ranoides could impact the placement of *T. servatus*.

**Equal Weight—**When using a topology inferred on the phylogeny of Jetz and Pyron (2018) as a constraint, we recovered 8 MPTs with a score of 1566 steps. The strict consensus (CI = 0.149, RI = 0.478) places *T. servatus* in a trichotomy with the two pyxicephalines (Fig. S7A). The clade is strongly supported by thirteen synapomorphies, including the presence of a contact between nasals and squamosals (11: 0–>1), the expension of the zygomatic ramus of the squamosals, allowing for its articulation with the maxillae (10: 1–>2), the presence of a distal expansion of the crista parotica (39: 0–>1) and the enclosement of the pathway for the

occipital artery into a canal (7: 0–>2; see Appendix S6 in Supplement Data 1 for the detailed list).

When using a topology inferred on the phylogeny proposed by Feng et al. (2017) as a constrain, we recovered 4 MPTs, with a score of 1562. In the strict consensus tree (CI = 0.151, RI = 0.486; Fig. S7B), *T. servatus* was recovered in the same position as with a topology inferred on the phylogeny of Jetz and Pyron (2018), in a trichotomy with the two pyxicephalinae taxa, supported by seventeen synapomorphies, thirteen of them recovered in the previous analysis, with an additional four, the partial ossification of the septum nasi of the nasal capsule (34:0–>1) , the ossification of the crista parotica (38: 0–>1), the translocation of the articulation between the lower jaw and the skull to a positon well posterior to occiput (61: 0–>2) and the presence of anterolateral processes on the hyoid plate (64: 0–>1; not scored for *T. servatus*).

**Implied weight (k = 7)—**When using implied weights, and using a topology inferred on the phylogeny of Jetz and Pyron (2018) as a constrain, we obtained one tree (CI = 0.151, RI = 0.485), with *T. servatus* still found within the Pyxicephalidae, as a sister-taxon to the extant Pyxicephalinae (Fig. 15, Fig. S8), a placement similar to the one found with low constant value (k = 3) using implied weighting (Fig. S4). This clade is well-supported bythe same thirteen synapomorphies recovered in the previous analysis constrained on the same topology.

When constraining the analysis using the topology inferred from the analysis of Feng et al. (2017), we also obtained one tree (CI = 0.151, RI = 0.486) fully resolved (Fig. S9). The position of *T. servatus* is identical as before, as the closest taxon to the Pyxicephalinae, well supported by the same thirteen synapomorphies.

**Discussion—**The various analyses confirm the placement of *Thaumastosaurus* within Ranoides, more precisely within Natatanura. This position is mainly justified by several postcranial characters, such as the ossified omosternum and non-overlapping coracoids. This placement highlights the importance of postcranial characters to diminish the impact of homoplasy found in the skull characters of anurans (Duellman et Trueb, 1994; Báez and Gómez, 2018) and to correctly asset the position of extinct taxa.

In almost every analysis, *T. servatus* is recovered as a sister-taxon to the Pyxicephalinae, or within this clade. This position is not only the result of convergence due to hyperossification, because *C. guentheri*, another hyperossified natatanuran is only recovered with *Thaumastosaurus* when using equal weight, when the the weight of homoplastic characters is not reduced. The synapomorphies supporting the clade Pyxicephalinae + *Thaumastosaurus* are in mainly related to hyperossification, but the clade has good Bremer and moderate bootstrap supports (Fig. 14B, 15, Fig. S3–9). In the constrained analysis, *Thaumastosaurus* is also placed within the Pyxicephalidae, a clade composed of Pyxicephalinae and Cacosterninae. However, no osteological synapomorphy is known for this clade, and its only putative synapomorphy, the presence of a medial lingual process on the tongue (Frost et al., 2006), is not known in *Thaumastosaurus*, as no organs nor internal soft tissues are known for this species.

Conversely, the Pyxicephalinae is supported by four morphological synapomorphies (Frost et al., 2006), as was already proposed by Clarke (1981). One of them, the presence of an occipital canal, was also recovered as a synapomorphy for this clade in our analyses, while another one, a well-developed ramus interior (medial ramus; Clarke, 1981) of the pterygoids overlapping the parasphenoid alae, is present on *Thaumastosaurus*. The other two synapomorphies for the clade are a well-developed zygomatic ramus (= lamella alaris + processus maxillaris) of the squamosals (longer than its ramus paroticus) articulated with the

maxillae and a cranial exostosis (sensu Trueb, 1973). Cranial exostosis in its typical state (a reticulate pattern of bone deposition, forming an ornamentation) is present only in Pyxicephalinae (in the Natatanura), as *C. guentheri* presents a modified pattern of exostosis, named casquing (Trueb, 1973). The articulated skulls attributed to *T. gezei* present a reticulated dermal bone ornamentation that can be considered as skull exostosis (Fig. 5, 6; Roček and Lamaud, 1995: fig 1–5; Rage and Roček, 2007: fig.1–6; Laloy et al., 2013: fig. 3), and possess large squamosals with a well-developed zygomatic ramus longer than its otic ramus, articulating with the maxillae, forming a closed bony lateral margin of the orbit (Fig. 5B). In addition, the presence of a contact between the zygomatic (lamella alaris) of the squamosals and the nasals is another character recovered in both extant pyxicephalinae and *T. gezei*, and not in *C. guentheri*.

*Thaumastosaurus servatus* shows all the synapomorphies of the Pyxicephalinae and is found in almost all analyses as the closest taxon to the pyxicephaline crown clade. It can therefore be confidently placed within Pyxicephalidae. Furthermore, we can consider *T. servatus* as a stem-Pyxicephalinae.

Several Cretaceous taxa were included in the analyses: *Baraubatrachus pricei, Eurycephalella alcinae, Arariphrynus placidoi, Beelzebufo ampinga*, *Uberabatrachus carvalhoi* and *Cratia gracilis.* Their position throughout the analyses are similar to the ones recovered in recent analyses (Báez and Gómez, 2018). *Baraubatrachus pricei* and *Eurycephalella alcinae* are recovered within the Autraslobatrachia, close to *Calyptocephalella gayi*. *Arariphrynus placidoi* is recovered within the Craugastoridae, but this position is poorly supported, as the taxon was in several analyses placed within various neobatrachian clades, even within the Ranoides, as a sister-taxa to the Afrobatrachia. This variability can be explained by the poorly known postcranial bones, especially around the pectoral girdle, where most critical characters for both Hyloides and Ranoides are found. *Cratia gracilis* is placed in

the same position as in previous analyses (Báez et al., 2009; Báez and Gómez, 2018). *U. carvalhoi* is recovered as a sister-taxon to the Ceratophryidae, a position that was also recovered in some analyses of Báez and Gómez (2018) but differs from the position they retained as their preferred one, as a sister-taxa to *B. ampinga* clustered within the Myobatrachia. *Beelzebufo ampinga* is recovered in various positions, but most often as a sister-taxon to all Ceratophryidae, a position proposed by previous analyses (Evans et al., 2008; Evans et al., 2014). However, this was challenged recently (Báez and Gómez, 2018) and the reasons for this uncertainty may be linked to the scarce post-cranial remains.

## PALEOBIOGEOGRAPHIC IMPLICATIONS

The fossil record of the Ranoides is scarce, with few fossils attributed to this clade, even fewer than to the Natatanura, prior to the Miocene (Gardner and Rage, 2016; Sanchiz, 1998). The few specimens are moreover mostly fragmentary remains (de Broin et al., 1974; Rage, 1984a; Roček and Lamaud, 1995; Báez and Werner, 1996). The molecular age for Ranoides has been estimated around 90.7 Ma (76.3 to 105.6 Ma, according to Frazão et al., 2015), during the Early to Late Cretaceous which is interesting given that the first remains attributed (putatively) to the clade are dated from the Cenomanian (between 100.5 Ma to 93.9 Ma; Báez and Werner, 1996; Marjanović and Laurin, 2014: fig. 4). However, these remains were neither described nor illustrated, making the validity of this attribution difficult to assess. The next putative remains are from the Santonian (86.3 Ma to 83.6 Ma) of In Beceten, Niger (de Broin et al., 1974; Rage,1984a) or from the Paleocene (66.0 to 56.0 Ma) from Cernay, France (Estes et al., 1967; Rage, 1984a). Geologically more recent remains clearly attributed to Ranoides are known in multiple sites during the Eocene and in the Quercy Phosphorites (Rage, 2016), with *T. gezei* and *T. bottii* (as well as other indeterminates forms; see Rage, 2016) as the best-known taxa.

For Natatanura, almost no fossil record is known, with *Thaumastosaurus* appearing to be the oldest undisputed known Natatanuran, as well as the oldest Ranoides with a valid taxon name (Sanchiz, 1998; Gardner and Rage, 2016; Rage, 2016). This is substantially more recent than the molecular age, around the transition Cretaceous/Paleocene, inferred in the most recent analysis (Feng et al., 2017)

The scarce record of Ranoides (including Natatanura) nevertheless provides useful data about the geographical origin of the clade: the African continent (Gardner and Rage, 2016). A large bias exists on the materials collected, as few fossil sites from Africa are known prior to the Pleistocene/Holocene (Gardner and Rage, 2016). However, new material has been published in the last decade, and the fossil record of various natatanuran clades is beginning to be documented.

The Natatanura (like the Ranoides) probably has an African origin, and some of the clades included in it also have a similar origin; they are still endemic to this continent nowadays (Gardner and Rage, 2016). The Pyxicephalidae is one of these clades. The attribution of *Thaumastosaurus*, an endemic clade of Western Europe (Vasilyan, 2018) to the Pyxicephalidae is at odd with its geographic range, limited to Sub-Saharan Africa (van der Meijden et al., 2011) for both extant and other extinct taxa (Gardner and Rage, 2016). In addition, *Thaumastosaurus* (Middle to Late Eocene, 40.5 to 33.5 Ma) is much older than the other fossils previously attributed to that clade (around 5.1 Ma for the most ancient specimen attributed; Gardner and Rage, 2016). This causes a large gap in both geographic and stratigraphic ranges and is even more surprising when considering that the clade origin lies in Africa according to all recent analyses (Bossuyt et al., 2006; Feng et al., 2017). This raises the possibility that although Pyxicephalidae have an African origin, the Pyxicephalinae (including *Thaumastosaurus*, as stem-Pyxicephalinae, see Phylogeny) may have originated in Western

Europe, during the Middle to Late Eocene, before their migration and diversification in South Africa.

However, two aspects have to be considered. First of all, the Pyxicephalidae diverged from its sister-clade around 60 Ma (Early to Middle Paleocene) according to recent molecular age (Feng et al. 2017). In this clade, the Pyxicephalinae has diverged from the Cacosterninae around 50 Ma (Hedges et al., 2015; Feng et al., 2017). The stratigraphic range for *Thaumastosaurus* is compatible with the molecular age for these various clades, as it is still younger. The second aspect is the scarce fossil record of the group in Africa. In the most recent review of the literature (Gardner and Rage, 2016), only seven sites have yielded fragmentary remains attributed to the Pyxicephalidae, none older than 5.1 Ma (Matthews et al., 2015), leaving a 45 Ma gap with the molecular age and 35 to 28 Ma with *Thaumastosaurus*. This gap in the fossil record shows that a large portion of the evolutionary history of the clade is undocumented in the fossil record, and it would not be surprising if new specimens from the Cenozoic of the continent were attributed to the clade, extending its geographic range and filling the stratigraphic gap with *Thaumastosaurus*. The inclusion of the latter taxon in the Pyxicephalidae, however, suggests that endemism of the clade arose only in more recent time. This might be linked to climate variations throughout the Cenozoic. A perhaps more likely alternative explanation is that the presence of *Thaumastosaurus* in Europe results from a dispersal event from Northern Africa when the climate in Europe was suitable for pyxicephalines.

We confirm the African affinities of *T. servatus*, proposed almost a decade earlier (Laloy et al., 2013), and we link this taxon to the faunistic exchange from Africa to Europe (Rage, 1984b; Gheerbrant and Rage, 2006) during the Palaeocene-Eocene thermal maximum (PETM) (Sluijs et al., 2006), possibly in latter half of this event, in the Early Eocene Climatic optimum (EECO). Starting in the Late Paleocene (Tanrattana et al., 2020), the temperature

increased (Sluijs et al., 2006; Bohaty et al., 2009) in Western Europe, and remained warm until the end of the Middle Eocene (Bohaty et al., 2009). During this period, Western Europe was characterized by a subtropical climate, with evergreen forest under warm and humid conditions (Escarguel et al., 2008; Héran et al., 2010; Tanrattana et al., 2020). During this period, a wave of new vertebrate taxa is recorded (Gheerbrant and Rage, 2006) in Western Europe. For the herpetofauna, this wave of immigration is recorded as soon as the Early Ecoene (MP7 accord to Rage, 2012), but could have began during the end of the Paleocene, with the arrival of several clade (e.g the Bufonidae, with the earliest record in Europe is during the Paleocene in Cernay; Rage, 2003). However, there are few sites from this period yielding amphibians or squamates remains (A. Folie, pers.com, 12/2020) and the origin of the new clades (for Europe) are still poorly known (e.g Blanidae or Pelobatidae; A. Folie pers.com, 12/2020). Still some clades have an origin that can be traced back to the African continent, that most likely immigrated from the isolated continent (Rage and Gheerbrant, 2020) throught an intermittent connection between African and Eurasia. These taxa, and the fauna they belong to, persited until the end of the Eocene.

At the end of the Eocene, a major cooling is recorded during the Eocene-Oligocene transition (EOT). This cooling is well recorded in numerous studies using different proxies (Escarguel et al., 2008; Héran et al., 2010; Lunt et al., 2017; Tanrattana et al., 2020) and is linked to the establishment of permanent ice caps on the Antarctica continent (Vandenberghe et al., 2012; Boscolo Galazzo et al., 2014). In Europe, the climate and environments dramatically changed. The climate became drier, with stronger seasonality and the appearance of a dry season (Escarguel et al., 2008; Tanrattana et al., 2020). The vegetation cover changed from forests to woodland savannah (Escarguel et al., 2008). This climate change probably triggered a moderate extinction event called the Grande Coupure (Stehlin, 1909), which has been particularly well-documented in mammals in Europe (Remy et al., 1987). Most of the

subtropical fauna of African origin disappeared and was replaced by Eurasian taxa adapted to temperate conditions. This event is also documented in the herpetofauna (Delfino et al., 2003; Rage, 2006, 2012; Macaluso et al., 2019). Among amphibians, *Thaumastosaurus* is the best-documented victim of this turnover; it disappeared from Western Europe around the end of the Eocene (Vasilyan, 2018).

## CONCLUSION

The tomography and study of the skeleton of the specimen QU17381, firstly described as the holotype of the bufonid *Bufo servatus*, yielded numerous data. The anatomical characters led to a new taxonomic attribution to the ranoid taxon *Thaumastosaurus servatus*. QU17381 is the third mummy from the Old Collections of the Quercy phosphorites attributed to this taxon, thus making it the best-known anuran in the Eocene of Western Europe.

Previous analyses placed *T. servatus* within the Natatanura, without specifying its position more precisely. Our analyses place *T. servatus* with the African hyperossified Pyxicephalinae, sharing a combination of skull features, as well as peculiar dermal ornamentation, and a contact between the squamosals and nasals which is unique within Natatanura and Ranoides. Constrained analyses confirmed this placement, as a sister-taxon to the extant Pyxicephalinae. This position is strengthened by the fact that the four synapomorphies diagnosing this clade in literature are present in *T. servatus*. This extinct taxon is probably a stem-Pyxicephalinae.

The position of *T. servatus* within the Natatanura and Pyxicephalinae provides new insights to calibrate molecular dating analyses, as it represents the oldest fossil record for Pyxicephalidae and Pyxicephalinae, previously known only from the Pliocene (around 5 My) and Pleistocene respectively. In addition, this is one of the few well-known taxa firmly attributed to the Natatanura in the Paleogene, with precise geological age. This also raises

questions on the geographic origin of Pyxicephalinae, as *T. servatus* extends the geological range of the clade of more than 33 My. Pyxicephalinae were previously considered to be distributed solely in Africa, whereas *T. servatus* is endemic to Western Europe. With *T. servatus* as a probable stem-Pyxicephalinae, the geographical range is greatly extended. The main biogeographical hypothesis is that the clade originated in Africa, and then migrated into Europe through dispersal of some natatanurans early in the Eocene, around the PETM, making *Thaumastosaurus* a member of the African herpetofauna present in Europe until the Eocene/Oligocene transition, when it was eliminated around the Grande Coupure (Delfino et al., 2003; Rage, 2006, 2012). However, given the scarce fossil record of Ranoides in Africa, especially during the Paleocene and Eocene, other hypotheses cannot be ruled out. Further findings could help to understand the evolution of this clade, which represents most speciose extant anuran taxon on the African continent.

## ACKNOWLEDGMENTS

We thank Damien Germain (CR2P, MNHN) for providing the access to historical specimens and Yves Laurent (MHNT) for the loan and information about the specimens from MNHT. We are grateful to Thierry Pélissié (Parc Naturel Régional des Causses du Quercy, France) and Mme. E. Cassan (grand daughter of the team leader of Escamps quarries) for sharing his knowledge on the Quercy region and sites on the search for the putative site of origin of the mummies. We thank Annemarie Ohler (MNHN) for bringing her expertise in nomenclature in the study of the nomenclatural history of *Bufo servatus* and other taxa named on the basis of the Quercy anuran mummies. We thank Diane Dosso (IBPC) and Pauline Prevost Marcihacy (IRHIS) for fruitful discussion and exchange on the history surrounding the mummies, bringing another angle into this mystery. We warmly thank Arnaud Mazurier

(IC2MP, Poitiers University) for supporting the whole tomographic acquisition process and advising on it. We are also grateful to Florent Goussard and Nathalie Poulet (CR2P, MNHN) for their help and advice on 3D reconstructions. This study was funded by a grant from the Fondation pour la Recherche sur la Biodiversité (FRB, Paris).

## REFERENCES

Aguilar, J.-P., S. Legendre, and J. Michaux. 1997. Actes du Congrès Biochrom'97 Montpellier 14-17 Avril. Biochronologie mammalienne du Cénozoïque en Europe et domaines reliés. Mémoires et Travaux de l'Institut de Montpellier de l'Ecole Pratique des Hautes Etudes 21, 1-181.

Anderson, M. A., and B. T. Miller. 2011. Early Iron Deposition in Teeth of the Streamside Salamander, *Ambystoma barbouri.* Journal of Herpetology 45:336–338.

Báez, A. M., and C. Werner. 1996. Presencia de Anuros Ranoideos en el Cretácico de Sudan. AMEGHINIANA 33:460.

Báez, A. M., and R. O. Gómez. 2018. Dealing with homoplasy: osteology and phylogenetic relationships of the bizarre neobatrachian frog *Baurubatrachus pricei* from the Upper Cretaceous of Brazil. Journal of Systematic Palaeontology 16:279–308.

Báez, A. M., G. J. B. Moura, and R. O. Gómez. 2009. Anurans from the Lower Cretaceous Crato Formation of northeastern Brazil: implications for the early divergence of neobatrachians. Cretaceous Research 30:829–846.

Biton, R., R. Boistel, R. Rabinovich, S. Gafny, V. Brumfeld, and S. Bailon. 2016. Osteological Observations on the Alytid Anura *Latonia nigriventer* with Comments on Functional

Morphology, Biogeography, and Evolutionary History. Journal of Morphology 277:1131–1145.

Bohaty, S. M., J. C. Zachos, F. Florindo, and M. L. Delaney. 2009. Coupled Greenhouse Warming and Deep-Sea Acidification in the Middle Eocene: Middle Eocene Warming and Ccd Shoaling. Paleoceanography 24:1–16.

Bolt, J. R., and R. E. Lombard. 1985. Evolution of the amphibian tympanic ear and the origin of frogs. Biological Journal of the Linnean Society 24:83–99.

Bonaparte, C. 1850. Conspectus Systematum. Herpetologiae et Amphibiologiae., Brill. Leiden, pp.

Boscolo Galazzo, F., E. Thomas, M. Pagani, C. Warren, V. Luciani, and L. Giusberti. 2014. The middle Eocene climatic optimum (MECO): A multiproxy record of paleoceanographic changes in the southeast Atlantic (ODP Site 1263, Walvis Ridge): MECO repercussions in the SE Atlantic. Paleoceanography 29:1143–1161.

Bossuyt, F., R. M. Brown, D. M. Hillis, D. C. Cannatella, and M. C. Milinkovitch. 2006. Phylogeny and Biogeography of a Cosmopolitan Frog Radiation: Late Cretaceous Diversification Resulted in Continent-Scale Endemism in the Family Ranidae. Systematic Biology 55:579–594.

Boulanger, G. A. 1886. Quelques mots en réponse à la note de M. Le Dr R. Blanchard sur la classification des Batraciens. Bulletin de la société zoologique de France 11:320–321.

Bremer, K. 1994. Branch support and Tree stability. Cladistics 10: 295–304.

de Broin, F., E. Buffetaut, J.-C. Koeniger, J. Rage, D. Russell, P. Taquet, C. Vergnaud-Grazzini, and S. Wenz. 1974. La faune de vertébrés continentaux du gisement d'In Beceten (Sénonien du Niger). Comptes Rendus de l'Académie des Sciences, Paris 279:439–472.

de Buffrénil, V., F. Clarac, A. Canoville, and M. Laurin. 2016. Comparative Data on the Differentiation and Growth of Bone Ornamentation in Gnathostomes (chordata: Vertebrata): Growth of Bone Ornamentation in Gnathostomes. Journal of Morphology 277:634–670.

de Buffrénil, V., F. Clarac, M. Fau, S. Martin, B. Martin, E. Pellé, and M. Laurin. 2015. Differentiation and Growth of Bone Ornamentation in Vertebrates: A Comparative Histological Study Among the Crocodylomorpha: Development of Bone Ornamentation in the Crocodylomorpha. Journal of Morphology 276:425–445.

Cameron, J. A., D. J. Milner, J. S. Lee, J. Cheng, N. X. Fang, and I. M. Jasiuk. 2012. Employing the Biology of Successful Fracture Repair to Heal Critical Size Bone Defects; pp. 113–132 in E. Heber-Katz and D. L. Stocum (eds.), New Perspectives in Regeneration. Current Topics in Microbiology and Immunology vol. 367. Springer Berlin Heidelberg, Berlin, Heidelberg.

Channing, A., and N. Baptista. 2013. *Amietia angolensis* and *A. fuscigula* (Anura: Pyxicephalidae) in southern Africa: A cold case reheated. Zootaxa 3640:501.

Channing, A., J. M. Dehling, Lötters, and R. Ernst. 2016. Species boundaries and taxonomy of the African river frogs (Amphibia: Pyxicephalidae: Amietia). Zootaxa 4155:1.

Clarke, B. T. 1981. Comparative Osteology and Evolutionary Relationships in the African Raninae (Anura: Ranidae). Monitore Zoologico Italiano. Supplemento 15:285–331.

Clemen, G. 1988. Experimental analysis of the capacity of dental laminae in *Ambystoma mexicanum* Shaw. Archives de biologie (Bruxelles) 99: 111–132.

Company, J., and Z. Szentesi. 2012. Amphibians from the Late Cretaceous Sierra Perenchiza Formation of the Chera Basin, Valencia Province, Spain. Cretaceous Research 37:240–245.

Congreve, C. R., and J. C. Lamsdell. 2016. Implied weighting and its utility in palaeontological datasets: a study using modelled phylogenetic matrices. Palaeontology 59:447–462.

Cope, E. D. 1864. On the Limits and Relations of the Raniformes. Proceedings of the Academy of Natural Sciences of Philadelphia 16:181–183.

Cross, R. 2017. The inside story on 20,000 vertebrates. Science 357:742–743.

Daudin, F. 1802. Histoire Naturelle des Rainettes, des Grenouilles et des Crapauds. de Bertrandet, Paris, 108 pp.

De Stefano, G. 1903. I Sauri del Quercy appartenenti alla colleztione Rossignol. Atti della Societa Italiana di Scienze Naturali 4:382–418.

Delfino, M., J. Rage, and L. Rook. 2003. Tertiary mammal turnover phenomena: what happened to the herpetofauna? DEINSEA 10:153–161.

Dubois, A., and A. Ohler. 2005. Taxonomic notes on the Asian frogs of the tribe Paini (Ranidae, Dicroglossinae): 1. Morphology and synonymy of *Chaparana aenea* (Smith, 1922), with proposal of a new statistical method for testing homogeneity of small samples. Journal of Natural History 39:1759–1778.

Duellman, W. E., and L. Trueb. 1994. Biology of Amphibians. JHU Press, 702 pp.

Duméril, C. 1805. Zoologie analytique, ou Méthode naturelle de classification des animaux, rendue plus facile à l'aide de tableaux synoptiques. Allais, 386 pp.

Dumont, M., T. Tütken, A. Kostka, M. J. Duarte, and S. Borodin. 2014. Structural and functional characterization of enamel pigmentation in shrews. Journal of Structural Biology 186:38–48.

Egawa, S., S. Miura, H. Yokoyama, T. Endo, and K. Tamura. 2014. Growth and differentiation of a long bone in limb development, repair and regeneration. Development, Growth & Differentiation 56:410–424.

Escarguel, G., S. Legendre, and B. Sigé. 2008. Unearthing deep-time biodiversity changes: The Palaeogene mammalian metacommunity of the Quercy and Limagne area (Massif Central, France). Comptes Rendus Geoscience 340:602–614.

Estes, R., Ma. Hecht, and R. Hoffstetter. 1967. Paleocene Amphibians from Cernay, France. American Museum Novitates 2295:1–25.

Evans, S. E., M. E. H. Jones, and D. W. Krause. 2008. A giant frog with South American affinities from the Late Cretaceous of Madagascar. Proceedings of the National Academy of Sciences 105:2951–2956.

Evans, S. E., J. R. Groenke, M. E. H. Jones, A. H. Turner, and D. W. Krause. 2014. New Material of *Beelzebufo*, a Hyperossified Frog (Amphibia: Anura) from the Late Cretaceous of Madagascar. PLoS ONE 9:e87236.

Fabrezi, M. 2006. Morphological evolution of Ceratophryinae (Anura, Neobatrachia). Journal of Zoological Systematics and Evolutionary Research 44:153–166.

Feng, Y.-J., D. C. Blackburn, D. Liang, D. M. Hillis, D. B. Wake, D. C. Cannatella, and P. Zhang. 2017. Phylogenomics reveals rapid, simultaneous diversification of three major clades of Gondwanan frogs at the Cretaceous–Paleogene boundary. Proceedings of the National Academy of Sciences 114:E5864–E5870.

Filhol, H. 1873. Sur des pièces fossiles provenant de batraciens, de lacertiens et d'ophidens, trouvés dans les dépôts de phosphates de chaux de l'Averyon. Comptes Rendus de l'Académie des Sciences, Paris 77:1556–1557.

Filhol, H. 1876. Sur les Reptiles fossiles des phosphorites du Quercy. Bulletin de La Société Philomathique de Paris 6:27–28.

Filhol, H. 1877. Recherches sur les phosphorites du Quercy: Etude des fossiles qu'on y rencontre et spécialement des mammifères, Librairie de l'Académie de médecine. Paris, 690 pp.

Frazão, A., H. R. da Silva, and C. A. de M. Russo. 2015. The Gondwana Breakup and the History of the Atlantic and Indian Oceans Unveils Two New Clades for Early Neobatrachian Diversification. PLOS ONE 10:e0143926.

Frost, D. R., T. Grant, J. Faivovich, R. H. Bain, A. Haas, C. F. B. Haddad, R. O. De Sá, A. Channing, M. Wilkinson, S. C. Donnellan, C. J. Raxworthy, J. A. Campbell, B. L. Blotto, P. Moler, R. C. Drewes, R. A. Nussbaum, J. D. Lynch, D. M. Green, and W. C. Wheeler. 2006. The Amphibian Tree of Life. Bulletin of the American Museum of Natural History 297:1–291.

Gardner, J. D., and J.-C. Rage. 2016. The fossil record of lissamphibians from Africa, Madagascar, and the Arabian Plate. Palaeobiodiversity and Palaeoenvironments 96:169–220.

Gèze, B. 1949. Les Gouffres à Phosphate du Quercy. Annales de Spéléologie 4:89–107.

Gheerbrant, E., and J.-C. Rage. 2006. Paleobiogeography of Africa: How distinct from Gondwana and Laurasia? Palaeogeography, Palaeoclimatology, Palaeoecology 241:224–246.

Goloboff, P. A. 1993. Estimating Character Weights During Tree Search. Cladistics 9:83–91.

Goloboff, P. A. 1997. Self-Weighted Optimization: Tree Searches and Character State Reconstructions under Implied Transformation Costs. Cladistics 13:225–245.

Goloboff, P. A., and J. S. Farris. 2001. Methods for Quick Consensus Estimation. Cladistics 17:S26–S34.

Goloboff, P. A., and S. A. Catalano. 2016. TNT version 1.5, including a full implementation of phylogenetic morphometrics. Cladistics 32:221–238.

Goloboff, P. A., A. Torres, and J. S. Arias. 2018a. Weighted parsimony outperforms other methods of phylogenetic inference under models appropriate for morphology. Cladistics 34:407–437.

Goloboff, P. A., J. M. Carpenter, J. S. Arias, and D. R. M. Esquivel. 2008. Weighting against homoplasy improves phylogenetic analysis of morphological data sets. Cladistics 24:758–773.

Goloboff, P. A., M. Pittman, D. Pol, and X. Xu. 2018b. Morphological Data Sets Fit a Common Mechanism Much More Poorly than DNA Sequences and Call Into Question the Mkv Model. Systematic Biology 68:494–504.

Gómez, R. O., and G. F. Turazzini. 2016. An overview of the ilium of anurans (Lissamphibia, Salientia), with a critical appraisal of the terminology and primary homology of main ilial features. Journal of Vertebrate Paleontology 36:e1030023.

Haas, A. 2003. Phylogeny of frogs as inferred from primarily larval characters (Amphibia: Anura). Cladistics 19:23–89.

Hedges, S. B., J. Marin, M. Suleski, M. Paymer, and S. Kumar. 2015. Tree of Life Reveals Clock-Like Speciation and Diversification. Molecular Biology and Evolution 32:835–845.

Héran, M.-A., C. Lécuyer, and S. Legendre. 2010. Cenozoic long-term terrestrial climatic evolution in Germany tracked by δ18O of rodent tooth phosphate. Palaeogeography, Palaeoclimatology, Palaeoecology 285:331–342.

Holman, J. A., and D. L. Harrison. 2002. A New *Thaumastosaurus* (Anura: Familia Incertae Sedis) from the Late Eocene of England, with Remarks on the Taxonomic and Zoogeographic Relationships of the Genus. Journal of Herpetology 36:621–626.

Holman, J. A., and D. L. Harrison. 2003. A new helmeted frog of the genus *Thaumastosaurus* from the Eocene of England. Acta Palaeontologica Polonica 48:157–160.

Jarošová, J., and Z. Roček. 1982. The Incrassatio Frontoparietalis in Frogs, its Origin and Phylogenetic Significance. Amphibia-Reptilia 3:111–124.

Jeanbernat, E. 1874. Procès-verbal de la séance du 6 février 1874; pp. 502–507 in Bulletin de la Société des Sciences Physiques et Naturelles de Toulouse. vol. 2.

Jetz, W., and R. A. Pyron. 2018. The interplay of past diversification and evolutionary isolation with present imperilment across the amphibian tree of life. Nature Ecology & Evolution 2:850–858.

Jones, A. S., and R. J. Butler. 2018. A new phylogenetic analysis of Phytosauria (Archosauria: Pseudosuchia) with the application of continuous and geometric morphometric character coding. PeerJ 6:e5901.

Kato, K., H. Nakagaki, Y. Sakakibara, J. A. Weatherell, and C. Robinson. 1988. The dissolution rate of enamel in acid in developing rat incisors. Archives of Oral Biology 33:657–660.

Laloy, F., J.-C. Rage, S. E. Evans, R. Boistel, N. Lenoir, and M. Laurin. 2013. A Re-Interpretation of the Eocene Anuran Thaumastosaurus Based on MicroCT Examination of a ‘Mummified’ Specimen. PLoS ONE 8:e74874.

Laurent, R. F. 1986. Sous Classe des Lissamphibiens (Lissamphiia) ; pp. 594–597 in Grassé P., and M. Delsol (edts), Traité de Zoologie, Anatomie, Systematique, Biologie. vol. 14. Paris.

Legendre, S., B. Marandat, B. Sigé, J.-Y. Crochet, M. Godinot, J.-L. Hartenberger, J. Sudre, M. Vianey-Liaud, B. Muratet, and J.-G. Astruc. 1992. Mammamlian fauna of Vielase (phosphorites of Quercy, in the South of France): paleontological evidence for karst formation in the Quercy area as early as the Early Eocene. Neues Jahrbuch für Geologie und Paläontologie - Monatshefte 1992:414–428.

Lunt, D. J., T. Dunkley Jones, M. Heinemann, M. Huber, A. LeGrande, A. Winguth, C. Loptson, J. Marotzke, C. D. Roberts, J. Tindall, P. Valdes, and C. Winguth. 2012. A model–data comparison for a multi-model ensemble of early Eocene atmosphere–ocean simulations: EoMIP. Climate of the Past 8:1717–1736.

Lynch, J. D. 1971.Evolutionary Relationships, Osteology and Zoogeography of Leptodactyloid Frogs. University of Kansas Museum of Natural History, Miscellaneous Publications 53: 1–238.

Lynch, J. D. 1973. The transition from archaic to advanced frogs; pp. 133–182 in J. L. Vial (ed.), Evolutionnary Biology of the Anurans. Contemporary resarch on major problems. University of Missouri Press.

Macaluso, L., J. E. Martin, L. Del Favero, and M. Delfino. 2019. Revision of the crocodilians from the Oligocene of Monteviale, Italy, and the diversity of European eusuchians across the Eocene-Oligocene boundary. Journal of Vertebrate Paleontology 39:e1601098

Marjanović, D., and M. Laurin. 2014. An updated paleontological timetree of lissamphibians, with comments on the anatomy of Jurassic crown-group salamanders (Urodela). Historical Biology 26:535–550.

Martín, C., M. A. Alonso-Zarazaga, and B. Sanchiz. 2012. Nomenclatural Notes on Living and Fossil Amphibians. Graellsia 68:159.

Matthews, T., E. van Dijk, D. L. Roberts, and R. M. H. Smith. 2015. An early Pliocene (5.1 Ma) fossil frog community from Langebaanweg, south-western Cape, South Africa. African Journal of Herpetology 64:39–53.

Mones A. 1989. Nomen Dubium vs Nomen Vanum. Journal of Vertebrate Paleontology 9: 232–234.

Nopcsa, D. F. B. 1908. Zur Kenntnis Der Fossilen Eidechsen. Beitrage zur Palaontologie und Geologie Osterreich-Ungarns und des Orients 21:34–62.

O'Reilly, J. E., M. N. Puttick, L. Parry, A. R. Tanner, J. E. Tarver, J. Fleming, D. Pisani, and P. C. J. Donoghue. 2016. Bayesian methods outperform parsimony but at the expense of precision in the estimation of phylogeny from discrete morphological data. Biology Letters 12:20160081.

Ősi, A., M. Szabó, H. Kollmann, M. Wagreich, R. Kalmár, L. Makádi, Z. Szentesi, and H. Summesberger. 2019. Vertebrate remains from the Turonian (Upper Cretaceous) Gosau Group of Gams, Austria. Cretaceous Research 99:190–208.

Paluh, D. J., E. L. Stanley, and D. C. Blackburn. 2020. Evolution of hyperossification expands skull diversity in frogs. Proceedings of the National Academy of Sciences 117:8554–8562.

Pélissié T., and B. Sigé (edts). 2006. 30 millions d'années de Biodiversité dynamique dans le paléokarst du Quercy. Strata 13:3–284.

Pereyra, M. O., M. C. Womack, J. S. Barrionuevo, B. L. Blotto, D. Baldo, M. Targino, J. J. Ospina-Sarria, J. M. Guayasamin, L. A. Coloma, K. L. Hoke, T. Grant, and J. Faivovich. 2016. The complex evolutionary history of the tympanic middle ear in frogs and toads (Anura). Scientific Reports 6:34130.

Poynton, J. C. 1964. The Amphibians of Southern Africa. Annals of the Natal Museum 17:1–334.

Piveteau, J.1927. Etudes sur quelques Amphibiens et Reptiles fossiles. Annales de Paléontologie 16 : 59–99.

Procter, M. J. B. 1919. On the Skull and Affinities of *Rana subsigillata* A. Dum. Proceedings of the Zoological Society of London 89:21–27.

Puttick, M. N., J. E. O'Reilly, A. R. Tanner, J. F. Fleming, J. Clark, L. Holloway, J. Lozano-Fernandez, L. A. Parry, J. E. Tarver, D. Pisani, and P. C. J. Donoghue. 2017. Uncertain-tree: discriminating among competing approaches to the phylogenetic analysis of phenotype data. Proceedings of the Royal Society B: Biological Sciences 284:20162290.

Pyron, R. A., and J. J. Wiens. 2011. A large-scale phylogeny of Amphibia including over 2800 species, and a revised classification of extant frogs, salamanders, and caecilians. Molecular Phylogenetics and Evolution 61:543–583.

Rage, J.-C. 1984a. La "Grande Coupure" Eocène/Oligocène et les herpétofaunes (Amphibiens et Reptiles): Problèmes du synchronisme des événements paléobiogéographiqes. Bulletin de la société géologique de France 26:1251–1257.

Rage, J.-C. 1984b. Are the Ranidae (Anura, Amphibia) known prior to the Oligocene? Amphibia-Reptilia 5:281–288.

Rage, J.-C. 2012. Oldest Bufonidae (Amphibia, Anura) from the Old World: a Bufonid from the Paleocene of France. Journal of Vertebrate Paleontology 23:462–463.

Rage, J.-C. 2006. The Lower Vertebrates from the Eocene and Oligocene of the Phosphorites du Quercy (france): An Overview. Strata 1:161–173.

Rage, J.-C. 2012. Amphibians and squamates in the Eocene of Europe: what do they tell us? Palaeobiodiversity and Palaeoenvironments 92:445–457.

Rage, J.-C. 2016. Frogs (Amphibia, Anura) from the Eocene and Oligocene of the Phosphorites du Quercy (France). An overview. Fossil Imprint 53–66.

Rage, J.-C., and E. Gheerbrant. 2020. Island Africa and Vertebrate Evolution: A Review of Data and Working Hypotheses; pp. 251-264 in Prasad, G.V.R. and P. Rajeev (edts), Biological

Consequences of Plate Tectonics: New Perspectives on Post-Gondwana Break-up. Springer, Cham, Switzerland.

Rage, J.-C., and Z. Roček. 2007. A new species of *Thaumastosaurus* (Amphibia: Anura) from the Eocene of Europe. Journal of Vertebrate Paleontology 27:329–336.

Reig, O. 1958. Proposiciones para una nueva macrosistemática de los anuros (nota preliminar). Physis 21:109–118.

Remy, J. A., J.-Y. Crochet, B. Sigé, J. Sudre, L. de Bonis, M. Vianey-Liaud, M. Godinot, J.-L. Hartenberger, B. Lange-Badré, and B. Comte. 1987. Biochronologie des phosphorites du Quercy : Mise à jour des listes fauniques et nouveaux gisements de mammifères fossiles. Münchner Geowissenschaftliche Abhandlungen A:169–188.

Rineau, V., R. Z. i Bagils, and M. Laurin. 2018. Impact of errors on cladistic inference: simulation-based comparison between parsimony and three-taxon analysis. Contributions to Zoology 87:25–40.

Rineau, V., A. Grand, R. Zaragüeta, and M. Laurin. 2015. Experimental systematics: sensitivity of cladistic methods to polarization and character ordering schemes. Contributions to Zoology 84:129–148.

Roček, Z. 1980. Cranial anatomy of frogs of the Family Pelobatidae Stannius, 1856, with outlines of their phylogeny and systematics. Acta Universitatis Carolinae - Biologica 3:1–164.

Roček, Z. 1994. Taxonomy and Distribution of Tertiary Discoglossids (anura) of The Genus *Latonia* V. Meyer, 1843. Geobios 27:717–751.

Roček, Z. 2008. The Late Cretaceous frog Gobiates from Central Asia: its evolutionary status and possible phylogenetic relationships. Cretaceous Research 29:577–591.

Roček, Z., and P. Lamaud. 1995. *Thaumastosaurus bottii* De Stefano, 1903, an anuran with Gondwanan affinities from the Eocene of Europe. Journal of Vertebrate Paleontology 15:506–515.

Roček, Z., and L. A. Nessov. 1993. Cretaceous Anurans from Central Asia. Palaeontographica Abteilung A 226:1–54.

Rose, F. L. 1968. Ontogenetic Changes in the Tooth Number of *Amphiuma Tridactylum*. Herpetologica 24: 182–184.

Sanchiz, B. 1998. Salientia. Dr. Friedrich Pfeil, Munich, 275 pp.

Scalia, F. 1976. Structure of the Olfactory and Accessory Olfactory Systems; pp. 213–233 in Frog Neurobiology. Springer Berlin Heidelberg, Berlin, Heidelberg.

Scott, E. 2005. A phylogeny of ranid frogs (Anura: Ranoidea: Ranidae), based on a simultaneous analysis of morphological and molecular data. Cladistics 21:507–574.

Sheil, C. A. 1999. Osteology and skeletal development of *Pyxicephalus adspersus* (Anura: Ranidae: Raninae). Journal of Morphology 240:49–75.

Sigé, B., J.-P. Aguilar, B. Marandat, and J. N.-G. Astruc. 1991. Extension au Miocène inférieur des remplissages phosphatés du Quercy. La Faune de Vertébrés de Crémat (Lot, France). Geobios 24:497–502.

Simon-Coincon R., and J. G. Astruc. 1991. Les pièges karstiques en Quercy : rôle et signification dans l'évolution des paysages. Bulletin de la société géologique de France 162 : 595–605.

Sluijs, A., S. Schouten, M. Pagani, M. Woltering, H. Brinkhuis, J. S. S. Damsté, G. R. Dickens, M. Huber, G.-J. Reichart, R. Stein, J. Matthiessen, L. J. Lourens, N. Pedentchouk, J. Backman, and K. Moran. 2006. Subtropical Arctic Ocean temperatures during the Palaeocene/Eocene thermal maximum. Nature 441:610–613.

Smith, T., and V. Codrea. 2015. Red Iron-Pigmented Tooth Enamel in a Multituberculate Mammal from the Late Cretaceous Transylvanian "Haţey Island". PLOS One 10(7):e0132550.

Špinar, Z. V. 1972. Tertiary Frogs from Central Europe. Academia, Prague; and Junk, The Hague, 463 pp.

Špinar, Z.V. 1978. *Latonia kolebabi* Špinar, 1976 (Amphibia) and remarks on the "genus Miopelobates". In Pokorny V. (ed.) Paleontologická konference 1977. Charles University, Prague: 289–303.

Stehlin, H. G. 1909. Remarques sur les faunules de mammifères des couches Eocène et Oligocène. Bulletin de La Société Géologique de France 9:488–520.

Suga, S., Y. Taki, and M. Ogawa. 1992. Iron in the Enameloid of Perciform Fish. Journal of Dental Research 71:1316–1325.

Tanrattana, M., A. Boura, F. M. B. Jacques, L. Villier, F. Fournier, A. Enguehard, S. Cardonnet, G. Voland, A. Garcia, S. Chaouch, and D. De Franceschi. 2020. Climatic evolution in Western Europe during the Cenozoic: insights from historical collections using leaf physiognomy. Geodiversitas 42:151.

Thevenin, A. 1903. Etude Géologique de la Bordure Sud-Ouest du Massif Central. Bulletin de la société géologique de France 14:353–555.

Tihen, J. 1962. A Review of New World Fossil Bufonids. The American Midland Naturalist 68: 1–50.

Tissier, J., J.-C. Rage, and M. Laurin. 2017. Exceptional soft tissues preservation in a mummified frog-eating Eocene salamander. PeerJ 5:e3861.

Tissier, J., J.-C. Rage, R. Boistel, V. Fernandez, N. Pollet, G. Garcia, and M. Laurin. 2016. Synchrotron analysis of a ‘mummified’ salamander (Vertebrata: Caudata) from the Eocene of Quercy, France: Exceptionally Preserved Fossil Urodele. Zoological Journal of the Linnean Society 177:147–164.

Trueb, L. 1973. Bones, Frogs and Evolution; pp. 65–133 in J. L. Vial (ed.), Evolutionary Biology of the Anurans. Contemporary Research on Major Problems. University of Missouri Press, Columbia.

Vandenberghe, N., F.J. Hilgen, R. P. Speijer, J. G. Ogg, F. M. Gradstein, O. Hammer, C. J. Hollis, and J. J. Hooker. 2012. The Paleogene Period; pp. 855-921 in F. Gradstein, J. Ogg, M. Schmitz, and G. Ogg (edts), The Geologic Time Scale. Elsevier.

Van der Meijden, A., A. Crottini, J. Tarrant, A. Turner, and M. Vences. 2011. Multi-locus phylogeny and evolution of reproductive modes in the Pyxicephalidae, an African endemic clade of frogs. African Journal of Herpetology 60:1–12.

Vasilyan, D. 2018. Eocene Western European endemic genus *Thaumastosaurus* : new insights into the question "Are the Ranidae known prior to the Oligocene?" PeerJ 6:e5511.

Submitted December,27th ,2020 ; revisions received Month DD, YYYY; accepted Month DD, YYYY

## FIGURE CAPTIONS

FIGURE 1. Geographical maps of potential localities for the mummies. **A**, map of France, with the Quercy region highlighted in black; **B**, map of the Quercy region showing the Aveyron part and neighboring lands in gray; **C**, close-up on the Aveyron area, modified from Gèze (1949), with the two-potential locations for sites that yielded the mummies in bold. Black dots indicate phosphorite quarries listed by Gèze (1949), gray squares indicate potential sites for the mummy series if Villeneuve is the putative area of origin, black arrow indicates the location of the site 'les Tempories', and transparent circle indicates the area of the Rosières sites.

FIGURE 2. External views of the specimen QU 17381, holotype of *Bufo servatus* in **A**, anterior; **B**, right lateral; **C**, posterior; **D**, left lateral; **E**, dorsal and **F**, ventral views. ? indicate the area previously identified as a parotoid gland. Black arrows on **B** and **D** indicate area

showing neat sub-millimetric folding preserved. **Abbreviations**: **nos**, nostril; **hum**, humerus; **spht**, sphenethmoid; **vert**, vertebrae; **urst**, urostyle. [planned for page width]

FIGURE 3. 3D-model of the specimen QU17381, holotype of *Bufo servatus*. **A**, dorsal view with the underlying bones in color by transparency; **B**, dorsal view of the sole osteological component; **C**, right antero-lateral view with the underlying bones in color; **D**, right antero-lateral view of the sole osteological component. **Abbreviations**: **ang**, angulosplenial; **exocpt**, exoccipital; **fp**, frontoparietals; **il**, ilium; **max**, maxilla; **nas**, nasal; **pect.gr**, pectoral girdle; **ptg**, pterygoid; **qdj**, quadratojugal; **spht**, sphenethmoid; **sql**, squamosal; **vert.col**, vertebral column.

FIGURE 4. External views of specimens QU 17279 and QU 17376. **A-C**, specimen QU 17279 in **A**, dorsal view; **B,** close-up on ridges and folds on the dorsally preserved skin; **C**, same specimen in left lateral view; **D**–**E**, specimen QU 17376 in **D**, dorsal; **E**, right lateral views. Black arrow indicates the are of potential tympanic membrane. **Abbreviations**: **eye**, eyeball; **nas.**, nasals.

FIGURE 5. Incomplete articulated skull of the mummy QU17381. Shown in **A,** dorsal; **B**, left lateral; **C**, palatal and **D**, posterior views**. Abbreviations**: **art.ocip,** foramen the arteria occipitalis canal; **crst.par**, crista parotica; **fp**, frontoparietals; **fo.mag**, foramen magnum; ; **gro.nas.duct**, groove for nasolacrimal duct; **qdj**, quadratojugal; **lam.al**, lamella alaris of the squamosal; **max**, maxilla; **m.choa**, margo choanalis of the vomer; **md.flg**, medial flange of

the squamosal; **med.pro**, medial process of the palatine; **nas**, nasal; **p.pstlat**, processus posterolateralis of the squamosal ; **pal**, palatine; **pro**, prootic; **parsh,** parasphenoid; **p.post**, processus posterior of the squamosal; **pr.dt.semcir.post**, prominentia ducti semicircularis posterioris; **p.prtocip**, processus prooticoccipitalis; **ptd**, pterygoid; **qjd**, quadratojugal; **r.ant**, ramus anterior of the pterygoid; **r. par**, ramus paroticus of the squamosal; **r.post**, ramus posterior of the pterygoid; **sphth**, sphenethmoid; **sql**, squamosal; **stp,** stapes; **vom**, vomer; **vom.teeth**, vomerine teeth.

FIGURE 6. Dermal bones from QU17381. **A**, frontoparietals in dorsal; **B**, ventral views; **C**, right squamosal in lateral view; **D**, right maxilla in lateral; **E**, medial views; **F**, right nasal in lateral view. Gray arrow points to the notch on the dorsal margin of the pars facialis of the maxilla; black arrow points to the notch on the frontoparietal. **Abbreviations**: **ant.sp**, anterior spine; **crst.dent**, crista dentalis; **dm.p.fa**, dorsal margin of the pars facialis of the maxilla; **fa.cerb.ant**, facies cerebralis anterior; **fa.cerb.post**, facies cerebralis posterior; **fos.max**, fossa maxillaris; **gro**, groove; **gro.nas.duct**, groove for nasolacrimal duct; **lam.al**, lamella alaris; **lam.ant**, lamina anterior; **lam.horz**, lamina horizontalis; **m.lat**, margo lateralis; **m.nas**, margo nasalis; **m.max,** margo maxillaris; **m.med**, margo medialis; **m.orb**, margo orbitalis of the squamosal and nasal; **pr.ant**, processus anterior; **pr.choan**, processus parachoanalis; **pr.cont**, pars contacta; **pr.lat**, processus lateralis; **pr.max**, processus maxillaris; **pr.front**, processus frontalis; **pr.paroc**, processus paraoccipitalis; **pr.paraorb**, processus paraorbitalis; **pr.post**, processus posterior of the maxilla and squamosal; **pr.postlat**, processus posterolateralis; **pr.ptd,** processus pterigoideus; **pr.zyg**, processus zygomatico-maxillaris; **res.vag**, recessus vaginiformis; **r.par**, ramus paroticus; **tect.suporb**, tectum supraorbitalis.

FIGURE 7. Suspensorium and Palate bones. **A**, left quadratojugal in lateral view; **B,** right angulosplenial in dorsal view; **C**, right palatine in ventral view; **D**, right vomer in dorsal view; **E**, parasphenoid in ventral view; **F**, left pterygoid in dorsal view. **Abbreviations**: **alae**, alae of the parasphenoid; **crst.prcord**, crista paracoronoidea; **crst.mad.ext**, crista mandibulae externa; **ext.spt**, extremitas spatulate; **lam.med**, lamina medialis; **m.choa**, margo choanalis; **med.pro**, medial process; **pr.ant**, processus anterior; **pr.ch.ant**, processus choanalis anterior; **pr.ch.post**, processus choanalis posterior; **pr.cord**, processus coronoideus; **pr.cult**, processus cultriformis; **pr.glnd,** processus glenoidalis; **pr.jug,** processus jugularis; **pr.max**, processus palatinus maxillae; **pr.post**, processus posterior; **m.max**, margo maxillaris; **m.med,** margo medialis; **m.post**, margo posterior; **r.ant**, ramus anterior; **r.int**, ramus interior; **r.post**, ramus posterior; **sul.cart.Meck**, sulcus cartilagine Meckeli; **sul.ptd**, sulcus pterygoideus; **tr.fa**, triangular facet.

FIGURE 8. Endocranial bones**. A-C**, sphenethmoid in **A**, dorsal; **B**, lateral and **C**, anterior views; **D-G**, prooticooccipital in **D**, posterior; **E**, dorsal; **F**, anterior and **G**, ventral views; **H**, left stapes in lateral view; **I**, right hyoid bone in dorsal view. **Abbreviations**: **cn.r.med.n.oph**, canalis ramus medialis nasalis ophthalmici; **con.occi**, condyle occipitalis; **crs.par**, crista parotica; **dor.exp**, dorsal ornamentation and exposure of the sphenthemoid; **dp**, depression anterior to the prominentia ducti semicircularis posterioris of the prooticoccipital; **fen.fp**, fenestra frontoparietalis; **fen.ov**, fenestra ovalis; **fo?**, foramen?; **fo.ju**, foramen jugaluris**,** **fo.mag**, foramen magnum, **fo.proot**, foramen prooticum, **fo.typ**, foramen tympanum; **ftp**, footplate; **gro**, groove; **gro.v.ju**, groove for vena jugularis; **l.suporb**, lamina supraorbitalis; **m.k**, median keel; **no**, notch; **occi**, occipital; **pr.lat**, processus lateralis; **pr.med.plt**, processus medialis plectri; **prom.d.sc.post**, prominentia ducti semicircularis posterioris; **sel.amp**, sella

amplificans; **sep.nas**, septum nasi; **sol.nas**, solum nasi; **tec.nas**, tectum nasi; **tect.synt**, tectum synotium.

FIGURE 9. Articulated diplasiocoelous vertebral column of the mummy QU17381, without the urostyle in **A**, dorsal; **B**, left lateral and **C**, ventral views. **Abbreviations**: **bic.cent**, biconcave centrum; **n.sp**, neural spine; **notch**, notch for ilium insertion; **postzyg**, postzygapophysis; **prezyg**, prezygapophysis; **sac.vt**, sacral vertebrae; **trans.pr**, transverse process.

FIGURE 10. Vertebral elements of the column. **A-B**, atlas in **A**, anterior and **B**, posterior views; **C-D**, sacral vertebrae in **C**, anterior and **D**, posterior views; **E-F,** urostyle in **E**, anterior and **F**, lateral views. **Abbreviations**: **ant.cd**, anterior condyle; **ant.ct**, anterior cotyles; **antdsl.pr**, anterodorsal process; **ant.l**, anterior lamina; **trans.pr**, transverse process; **cr.dor**, carina dorsalis; **cond**, condyle; **cv.cot**, cervical cotyles; **dl**, diapophyseal lamina; **fo.sp**; foramen spineal; **n.cl**, neural canal; **n.sp**, neural spine; **post.cd**, posterior condyles; **post.l**, posterior lamina; **postzyg**, postzygapophysis; **prezyg**, prezygapophysis.

FIGURE 11. Articulated pectoral girdle of QU17381 in ventral view. **Abbreviations**: **cl**, clavicle; **clth**, cleithrum; **cor**, coracoid; **omst**, omosternum; **scp**, scapula; **ster**, sternum.

FIGURE 12. Elements of the pectoral girdle. **A-B**, right scapula in **A,** medial and **B,** posterior views; **C**, right coracoid in dorsal view; **D-E**, left coracoid in **D,** ventral and **E,** medial views; **F-G**, left cleithrum in **F** lateral and **G,** medial views; **H**, right clavicle in dorsal view; **I**, sternum in dorsal view; **J**, omosternum in dorsal view. **Abbreviations**: **cal**, callus; **ext.med**, extremitas medialis; **glnd.fos**, glenoid fossa; **lam.ret**, lamina recurvata; **m.ant**, margo anterior; **m.drs**, margo dorsalis; **m.post**, margo posterior; **m.scp**, margo scapularis; **m.vert**, margo vertebralis; **med.crst**, medial crest; **p.acrm**, processus acromialis; **p.epcd**, processus epicoracoidalis, **p.glnd**, processus glenoidalis; **pr.ant**, processus anterior; **rm.ant**, ramus anterior; **s.intglnd**, sinus interglenoidalis; **sul.cart.parcord**, sulcus cartilagine praecoracoidealis.

FIGURE 13. Humerus and Ilium of QU17381**. A**, left humerus in lateral view; **B**, right ilium in lateral view. **Abbreviations**: **crst.vt**, crista ventralis; **dl.crst**, dorsal crest; **prox.head**, proximal head.

FIGURE 14. Reduced consensus trees from two analysis**. A**, Simplified strict consensus of 90 MPTs of 1373 steps (CI: 0.137, RI: 0.422) from the analysis under equal weight (EW), multistate characters ordered; **B**, Simplified strict consensus of 2 MPTs of 67 steps (CI = 0.168, RI = 0.548) from the analysis under implied weight (IW) with k = 7, multistate characters ordered. The † symbol identifies extinct taxa, the red area represents hyperossified ranoid taxa, the blue area represents the "Ranoides", the yellow area represents the clade Afrobatrachia + *Arariphrynus placidoi*, the brown area represents the microhylids. Numbers above branches designate Bremer support; numbers below branches are bootstrap frequencies.

FIGURE 15. Simplified MPT from a constrained analysis**.** Reduced MPT of 72 steps (CI = 0.151, RI = 0.485) from the constrained analysis using a molecular scaffold tree from Jetz and Pyron 2018, performed under IW with k = 7, multistate characters ordered. The † symbol identifies extinct taxa. Numbers above branches designate Bremer support; numbers below branches are bootstrap frequencies.

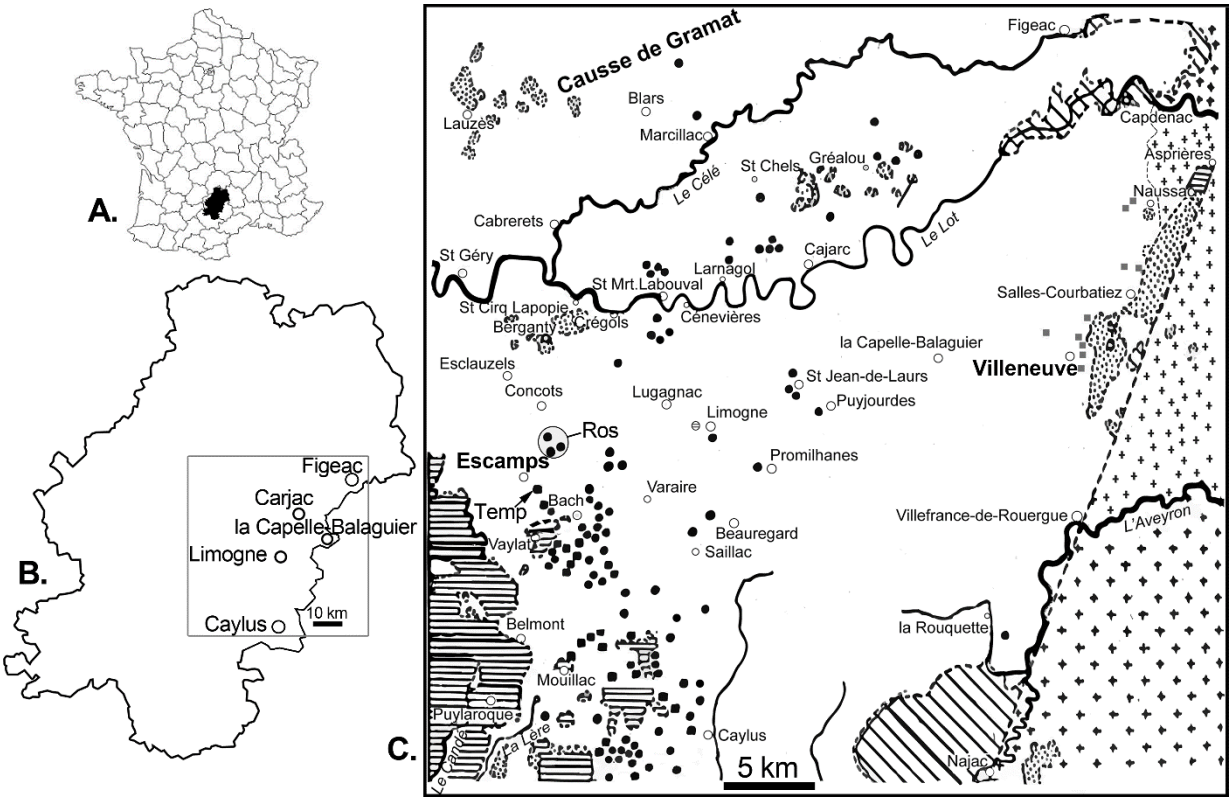

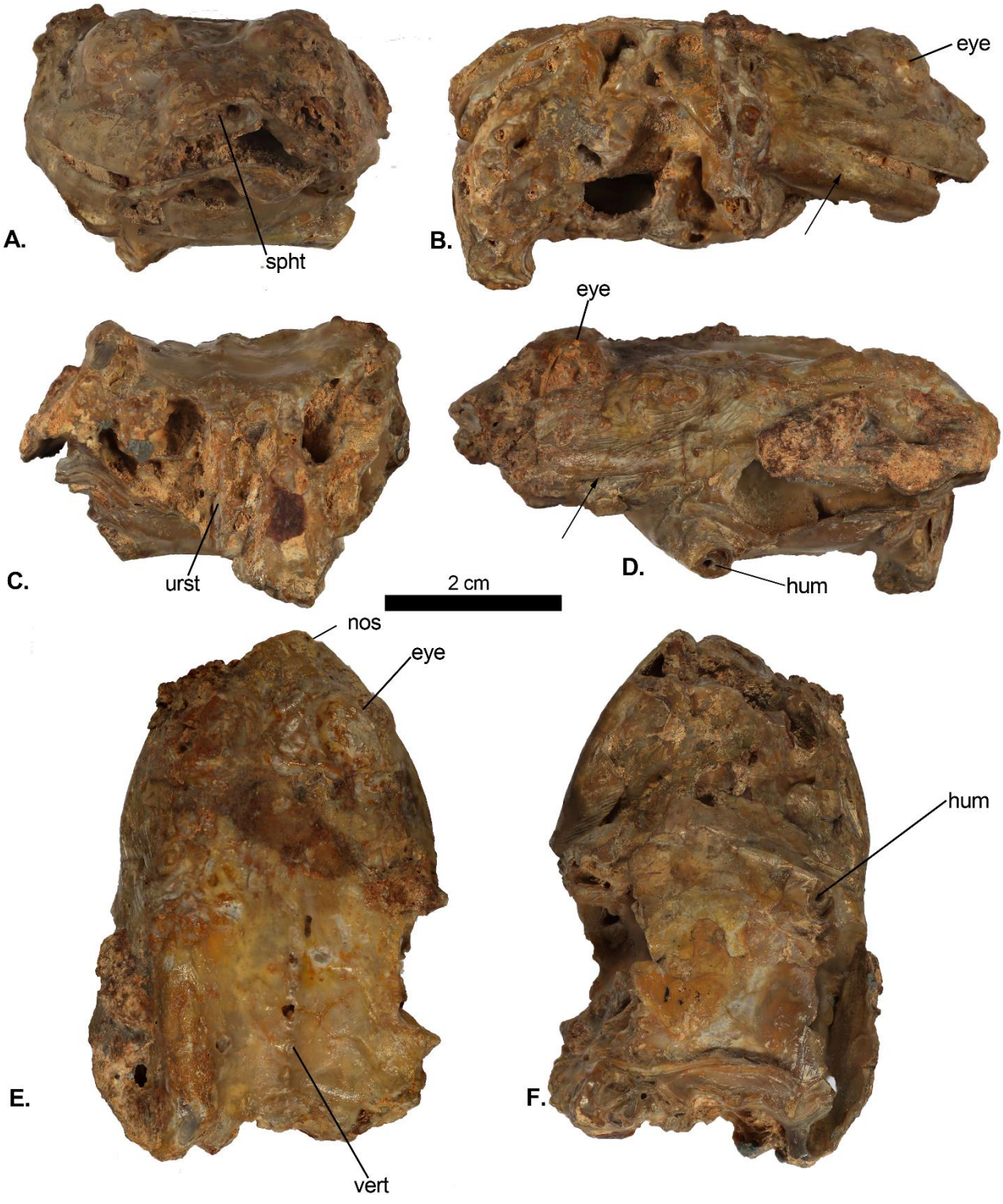
A.
spht
B.
eye
C.
urst
eye
D.
hum
2 cm
nos
eye
E.
vert
F.
hum

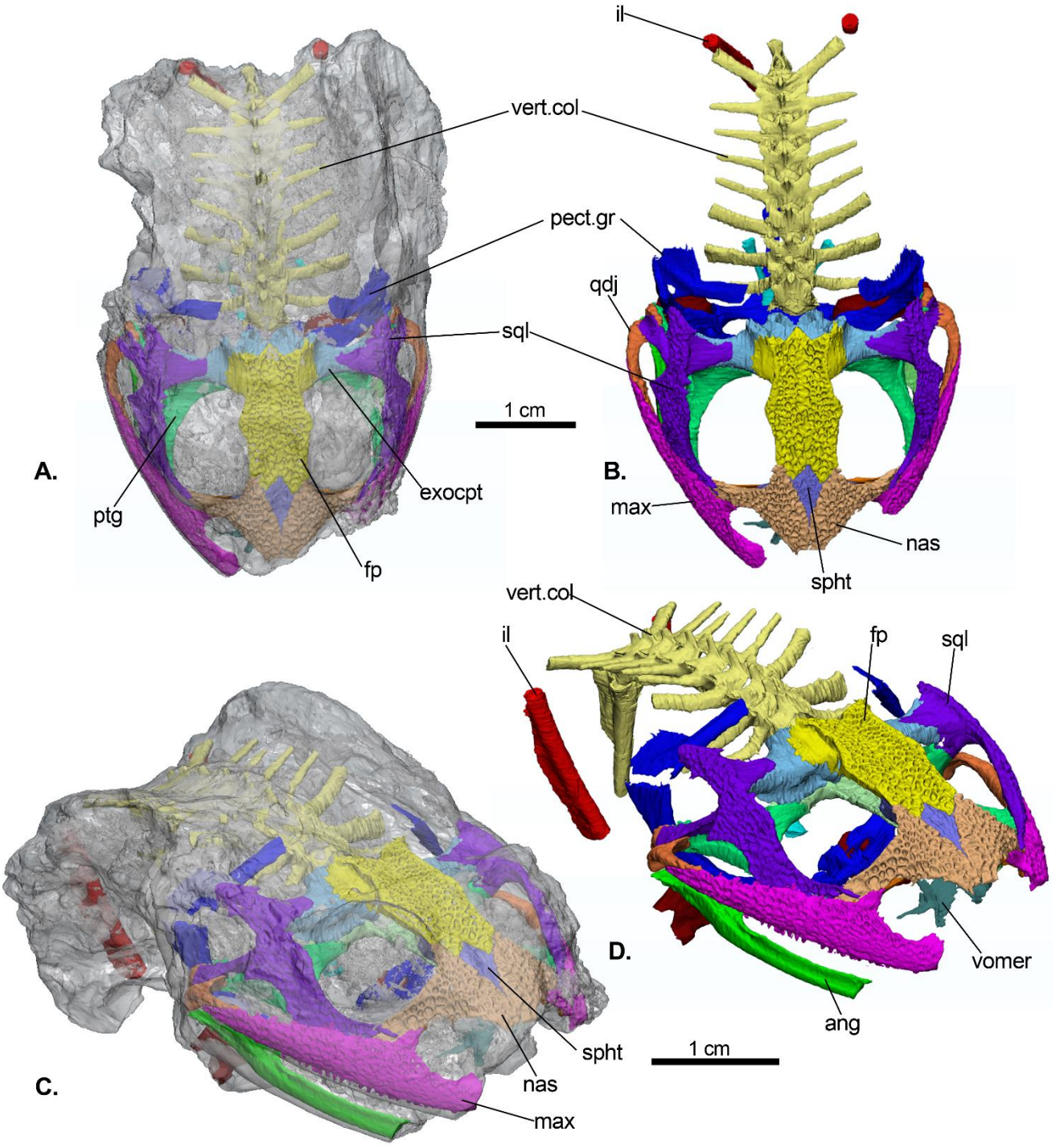
A.
vert.col
pect.gr
sql
1 cm
ptg
exocpt
fp
B.
il
qdj
max
nas
spht
C.
spht
nas
max
D.
vert.col
il
fp
sql
vomer
ang
1 cm

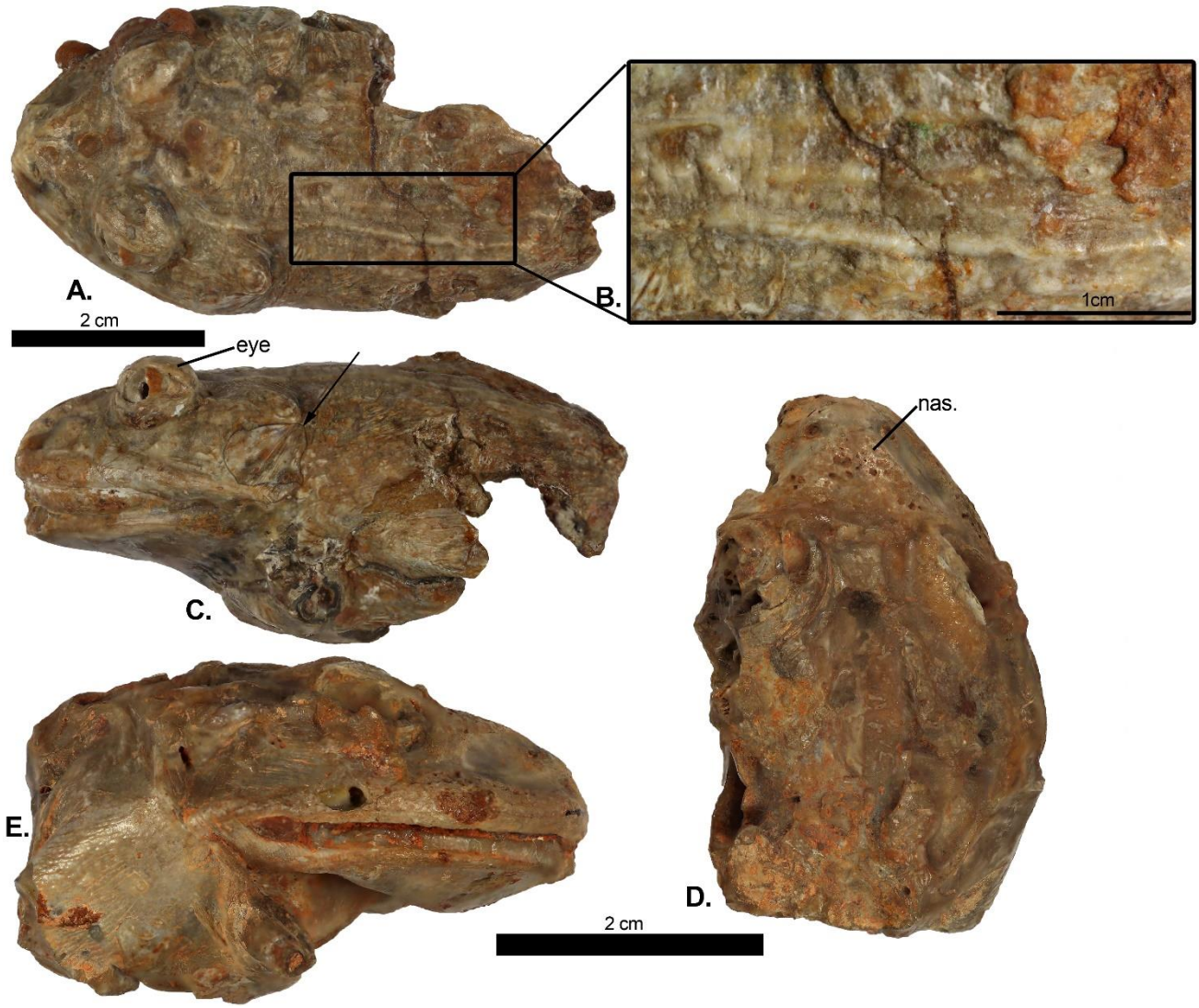
A.
2 cm
B.
1cm
eye
C.
nas.
D.
E.
2 cm

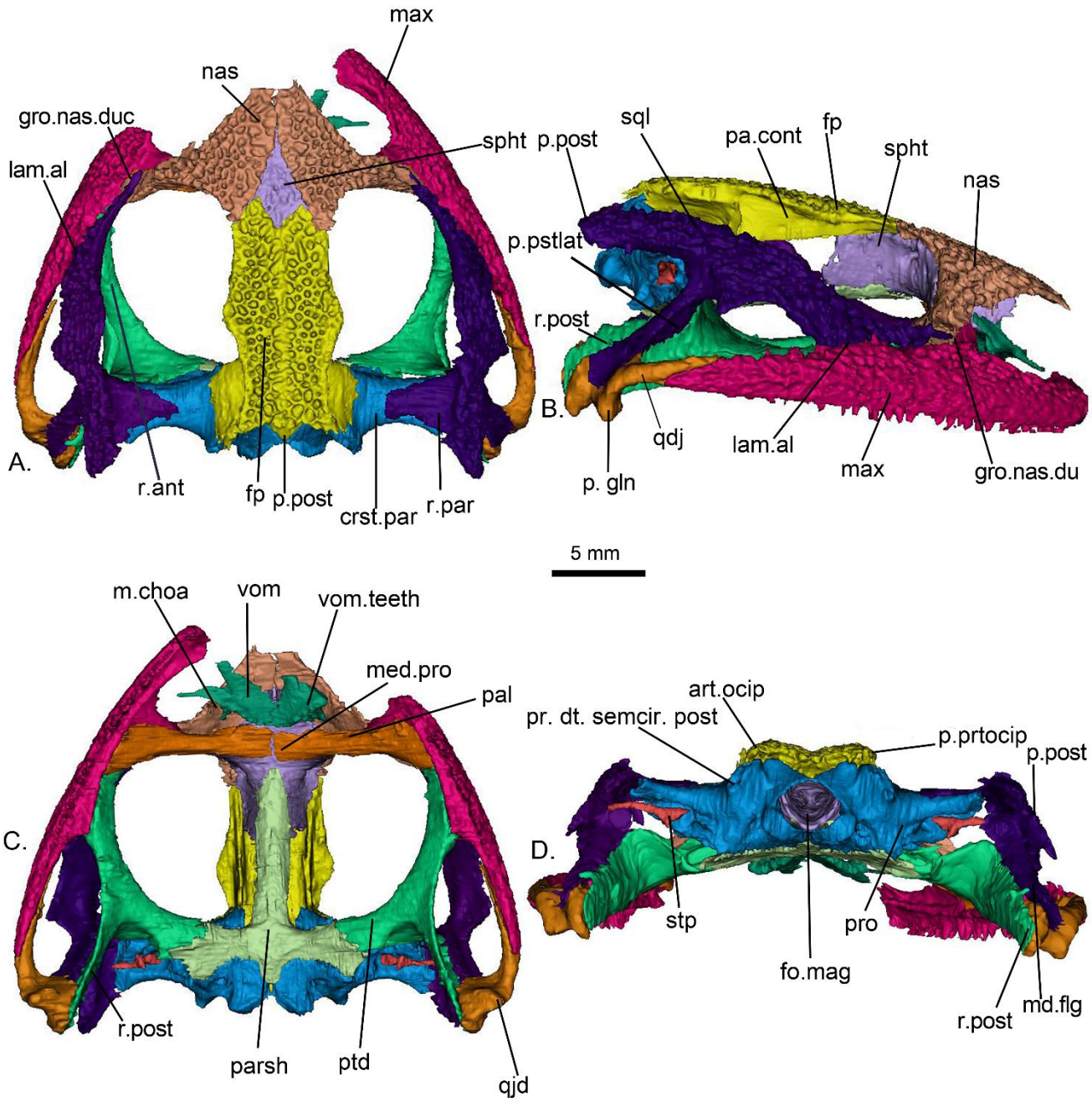
max
nas
gro.nas.duc
spht
lam.al
A.
r.ant
fp
p.post
crst.par
r.par
sql
p.post
pa.cont
fp
spht
nas
p.pstlat
r.post
B.
qdj
lam.al
max
gro.nas.du
p. gln
5 mm
m.choa
vom
vom.teeth
med.pro
pal
C.
r.post
parsh
ptd
qjd
art.ocip
pr. dt. semcir. post
p.prtocip
p.post
D.
stp
pro
fo.mag
r.post
md.flg

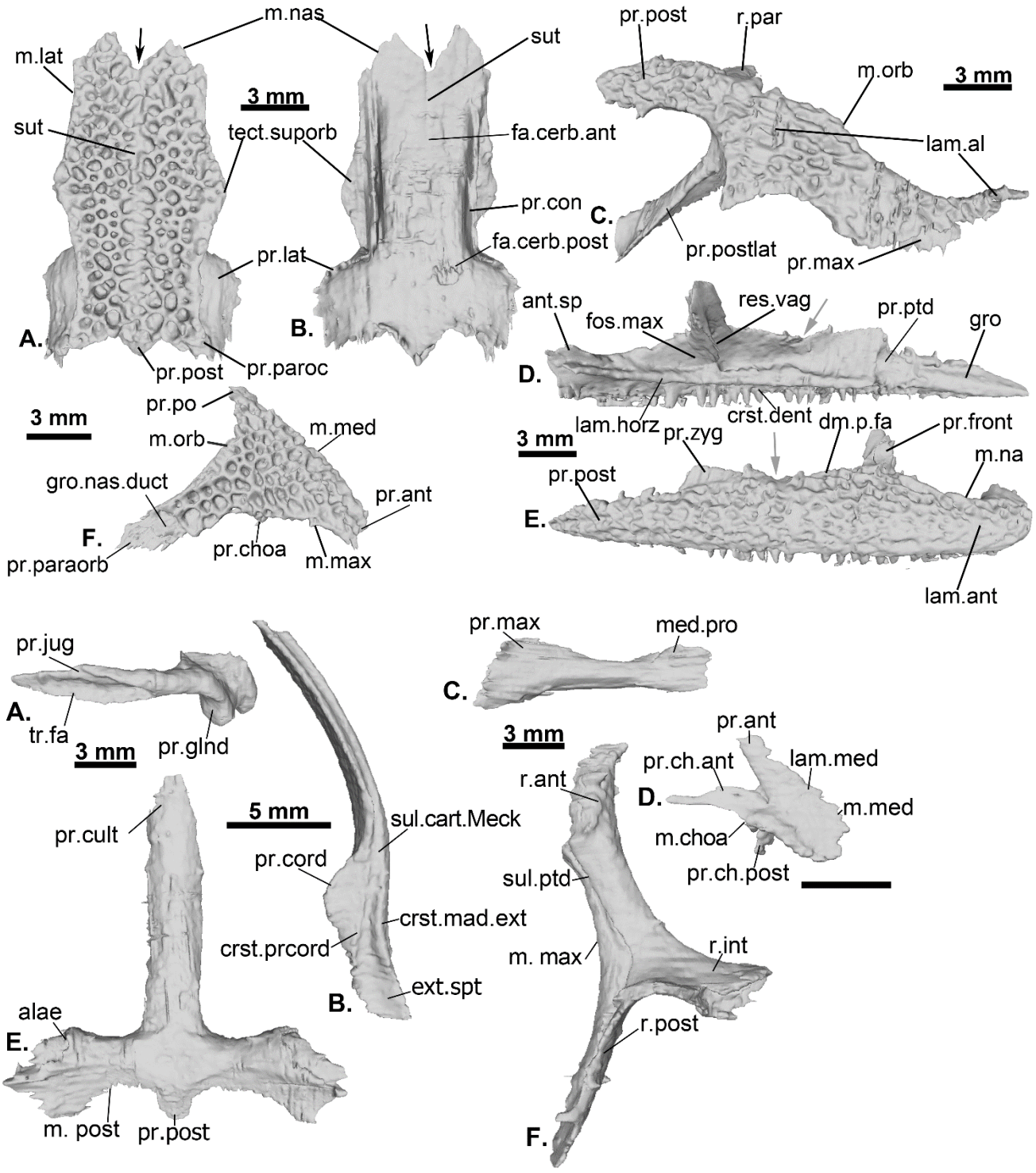
m.nas
m.lat
sut
3 mm
tect.suporb
pr.lat
A.
pr.post
pr.paroc
sut
fa.cerb.ant
pr.con
fa.cerb.post
B.
pr.post
r.par
m.orb
3 mm
lam.al
C.
pr.postlat
pr.max
ant.sp
fos.max
res.vag
pr.ptd
gro
D.
lam.horz
pr.zyg
crst.dent
dm.p.fa
pr.front
3 mm
m.na
pr.post
E.
lam.ant
pr.po
m.orb
m.med
gro.nas.duct
pr.ant
F.
pr.choa
m.max
pr.paraorb
pr.jug
A.
tr.fa
3 mm
pr.glnd
pr.max
med.pro
C.
3 mm
pr.ant
pr.ch.ant
lam.med
r.ant
D.
m.med
m.choa
pr.ch.post
pr.cult
5 mm
sul.cart.Meck
pr.cord
crst.mad.ext
crst.prcord
ext.spt
B.
sul.ptd
m. max
r.int
r.post
alae
E.
m. post
pr.post
F.

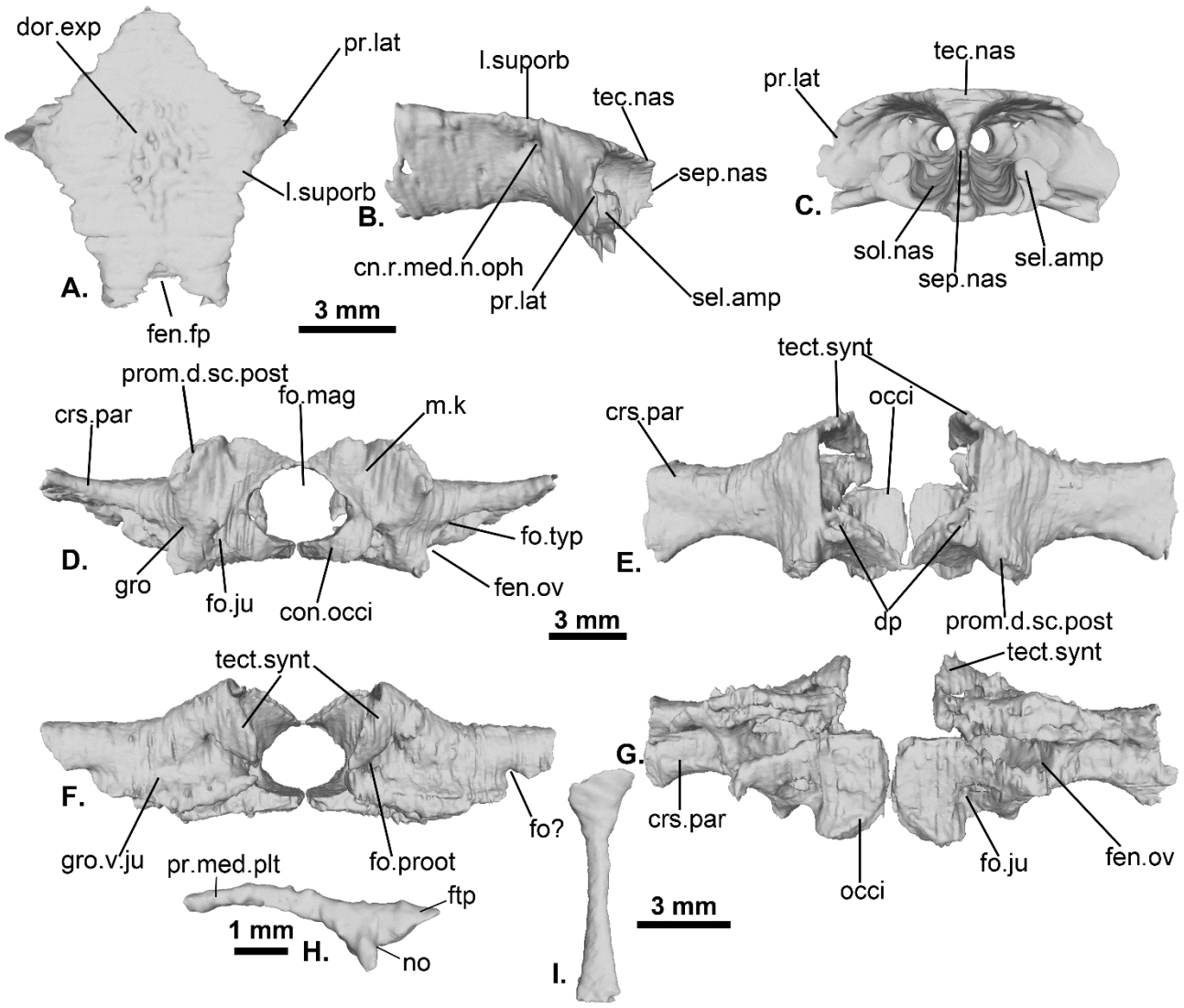
dor.exp
pr.lat
l.suporb
A.
fen.fp
3 mm
l.suporb
tec.nas
sep.nas
B.
cn.r.med.n.oph
pr.lat
sel.amp
tec.nas
pr.lat
C.
sol.nas
sep.nas
sel.amp
prom.d.sc.post
crs.par
fo.mag
m.k
D.
gro
fo.ju
con.occi
fo.typ
fen.ov
3 mm
tect.synt
occi
crs.par
E.
dp
prom.d.sc.post
tect.synt
F.
gro.v.ju
pr.med.plt
fo.proot
fo?
ftp
1 mm
H.
no
I.
G.
crs.par
occi
fo.ju
fen.ov
3 mm

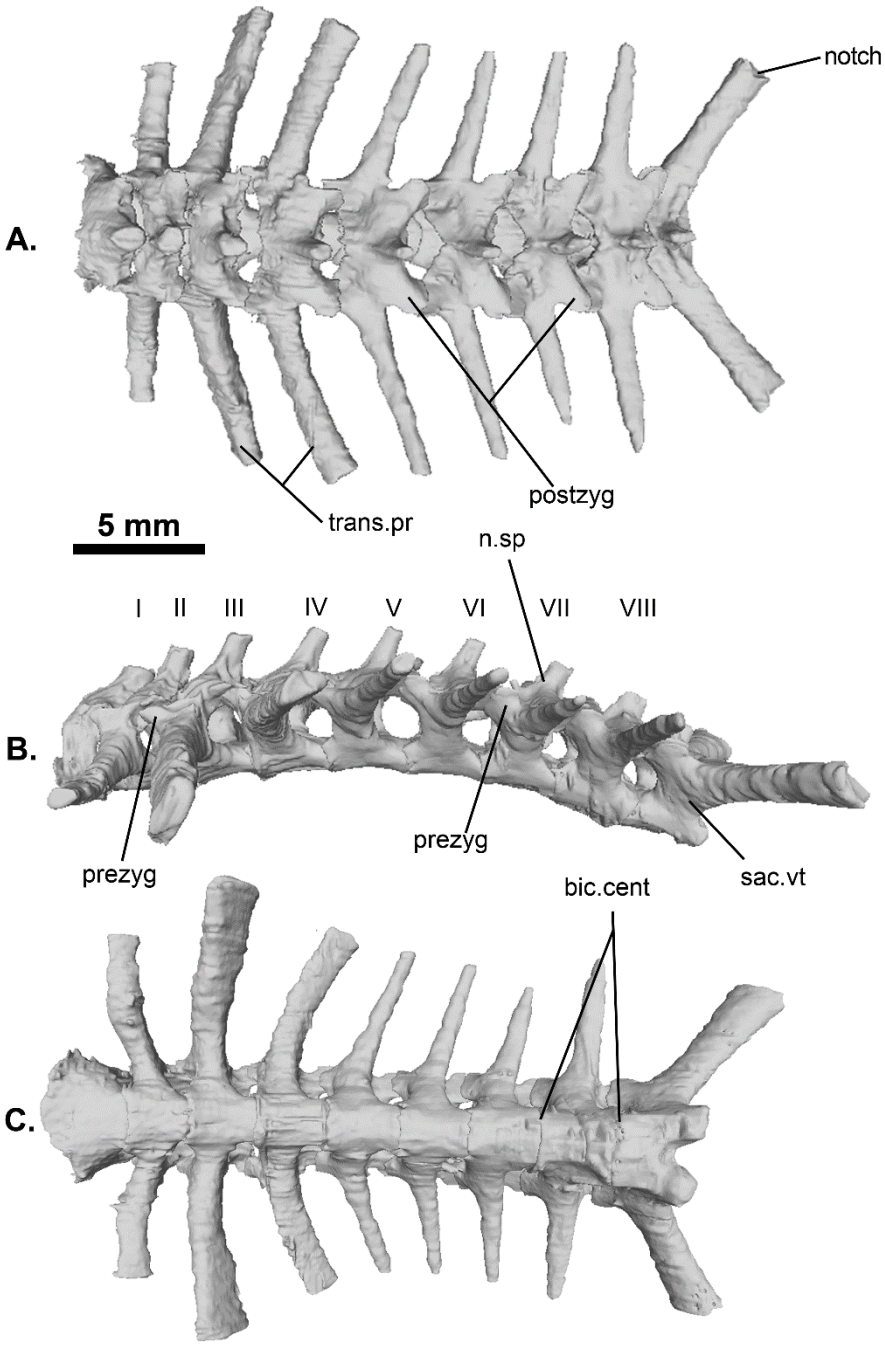
A.
notch
postzyg
trans.pr
5 mm
B.
n.sp
I
II
III
IV
V
VI
VII
VIII
prezyg
prezyg
sac.vt
C.
bic.cent

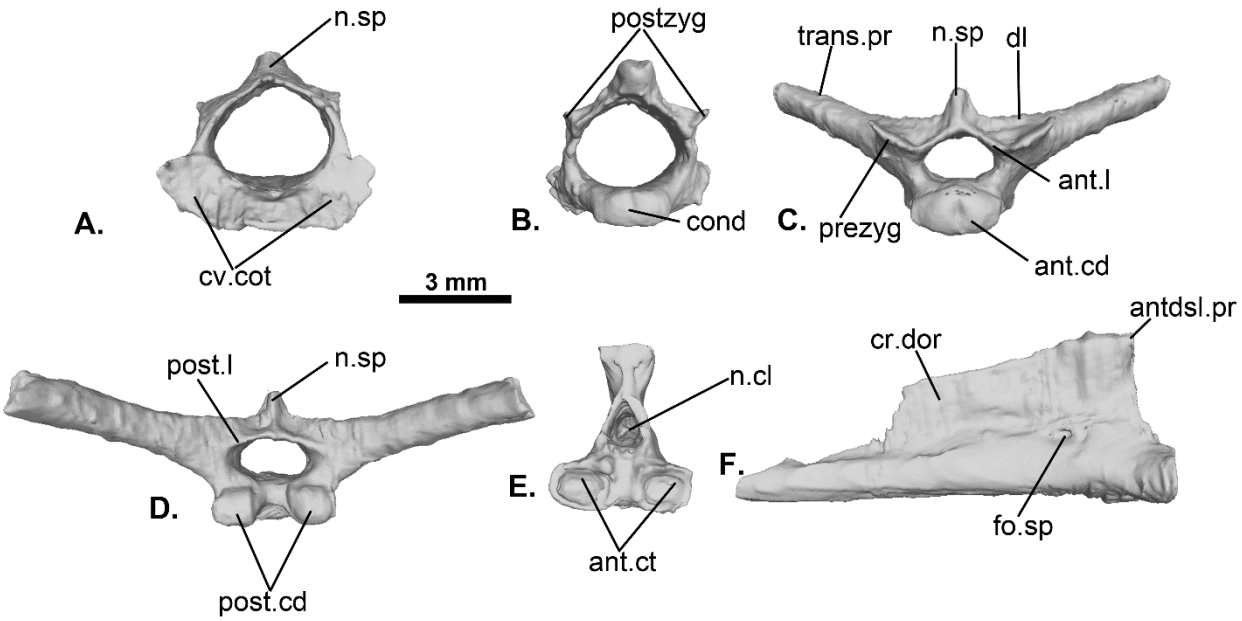
A.
n.sp
cv.cot
3 mm
B.
postzyg
cond
C.
trans.pr
n.sp
dl
ant.l
prezyg
ant.cd
D.
post.l
n.sp
post.cd
E.
n.cl
ant.ct
F.
antdsl.pr
cr.dor
fo.sp

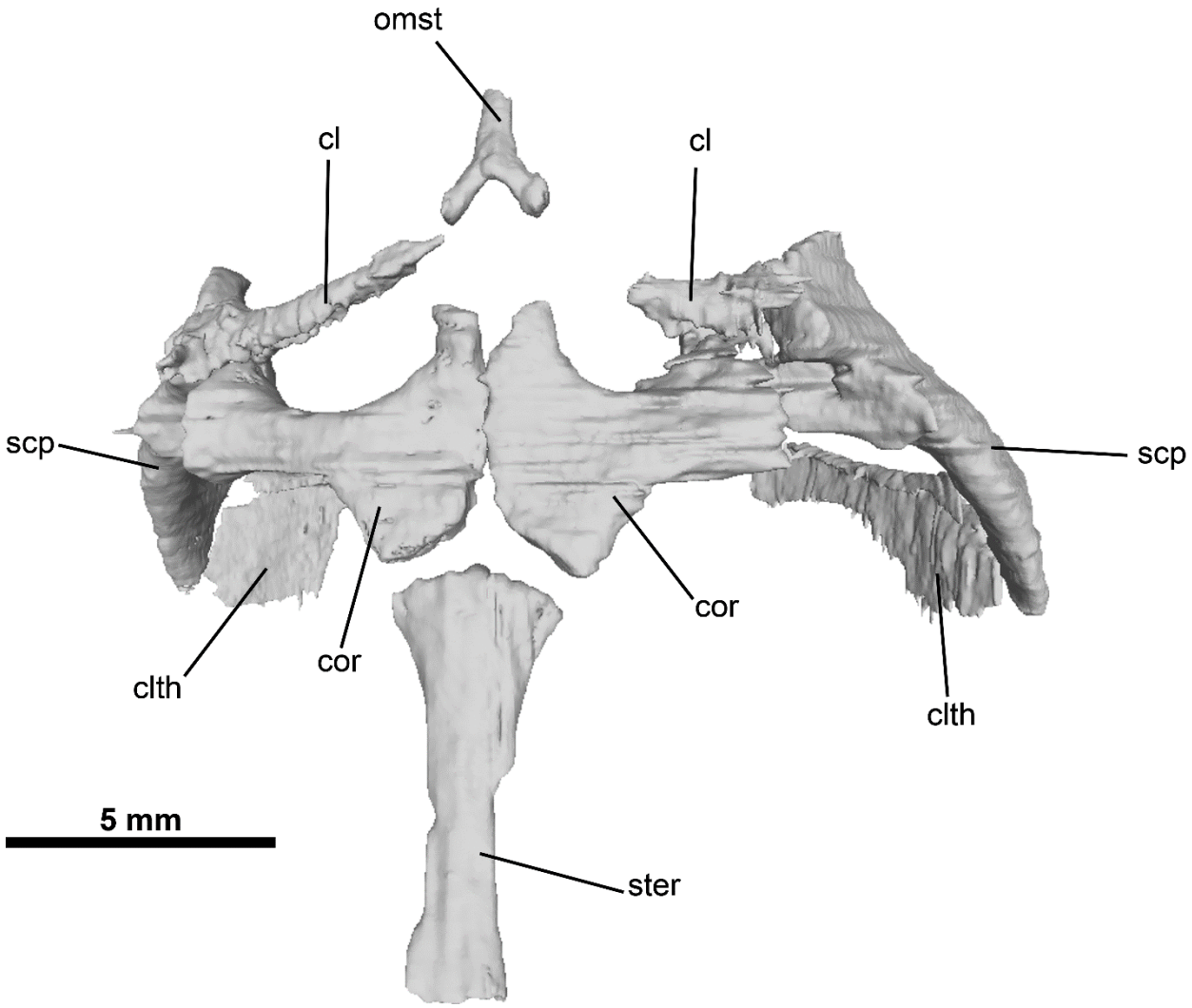
omst
cl
cl
scp
scp
cor
cor
clth
clth
5 mm
ster

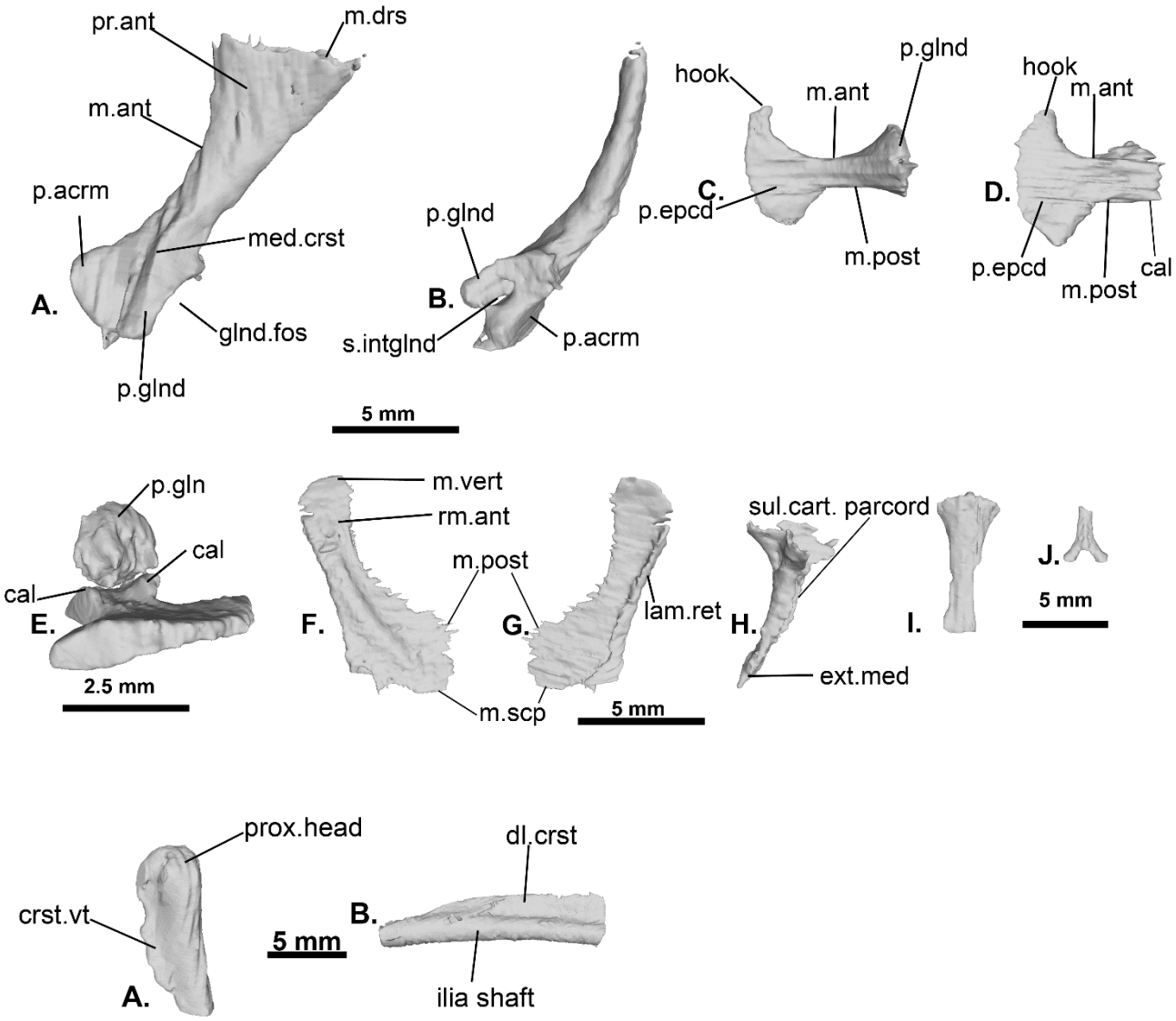
pr.ant
m.drs
m.ant
p.acrm
med.crst
A.
glnd.fos
p.glnd
5 mm
p.glnd
B.
s.intglnd
p.acrm
hook
p.glnd
m.ant
C.
p.epcd
m.post
hook
m.ant
D.
p.epcd
cal
m.post
p.gln
cal
cal
E.
2.5 mm
m.vert
rm.ant
m.post
F.
G.
lam.ret
m.scp
5 mm
sul.cart. parcord
H.
ext.med
I.
J.
5 mm


prox.head
crst.vt
A.
5 mm
dl.crst
B.
ilia shaft

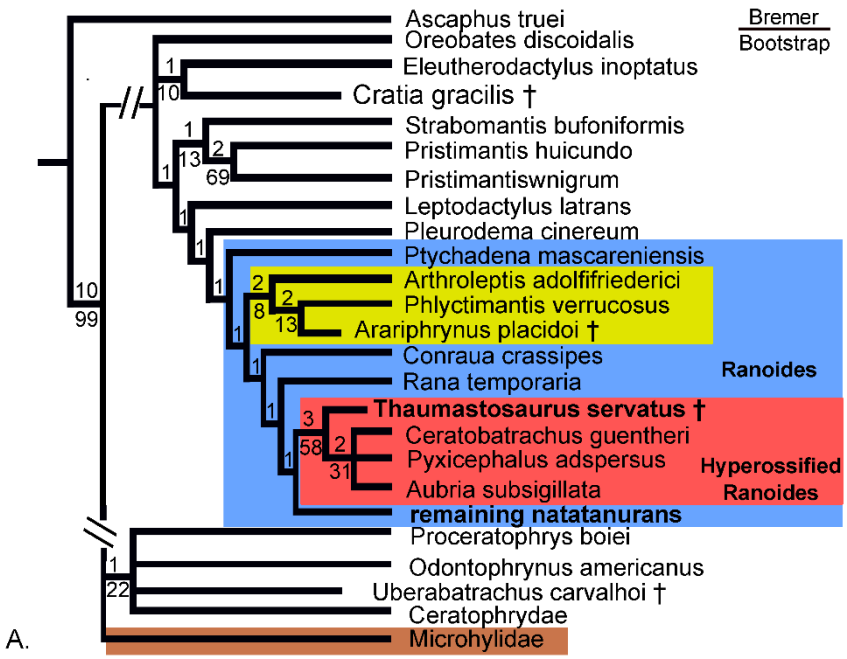
Bremer
Bootstrap
Ascaphus truei
Oreobates discoidalis
Eleutherodactylus inoptatus
Cratia gracilis †
Strabomantis bufoniformis
Pristimantis huicundo
Pristimantiswnigrum
Leptodactylus latrans
Pleurodema cinereum
Ptychadena mascareniensis
Arthroleptis adolfifriederici
Phlyctimantis verrucosus
Arariphrynus placidoi †
Conraua crassipes
Rana temporaria
Ranoides
Thaumastosaurus servatus †
Ceratobatrachus guentheri
Pyxicephalus adspersus
Aubria subsigillata
Hyperossified Ranoides
remaining natatanurans
Proceratophrys boiei
Odontophrynus americanus
Uberabatrachus carvalhoi †
Ceratophrydae
Microhylidae
A.

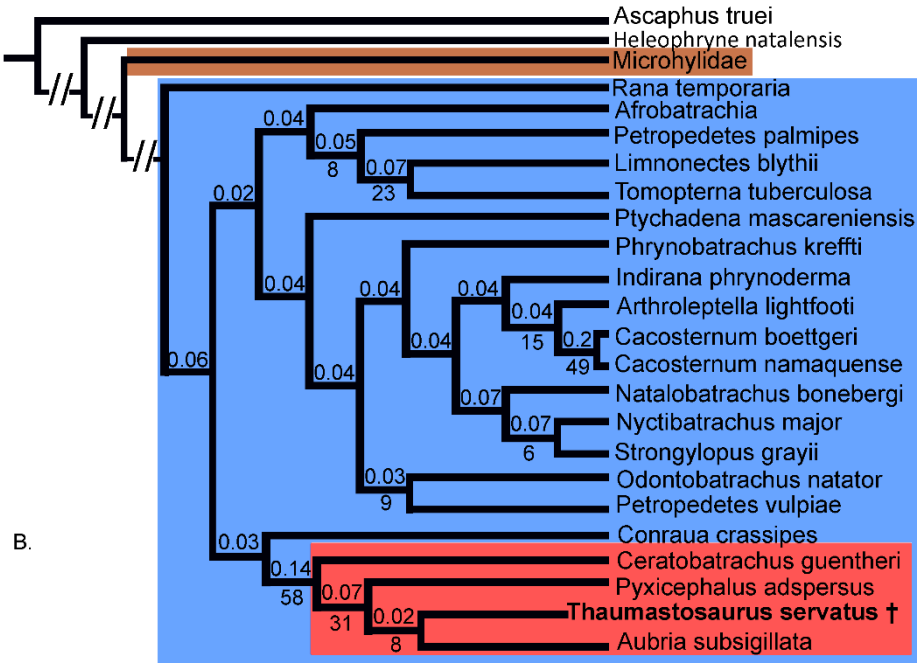
Ascaphus truei
Heleophryne natalensis
Microhylidae
Rana temporaria
Afrobatrachia
Petropedetes palmipes
Limnonectes blythii
Tomopterna tuberculosa
Ptychadena mascareniensis
Phrynobatrachus kreffti
Indirana phrynoderma
Arthroleptella lightfooti
Cacosternum boettgeri
Cacosternum namaquense
Natalobatrachus bonebergi
Nyctibatrachus major
Strongylopus grayii
Odontobatrachus natator
Petropedetes vulpiae
Conraua crassipes
Ceratobatrachus guentheri
Pyxicephalus adspersus
Thaumastosaurus servatus †
Aubria subsigillata
B.

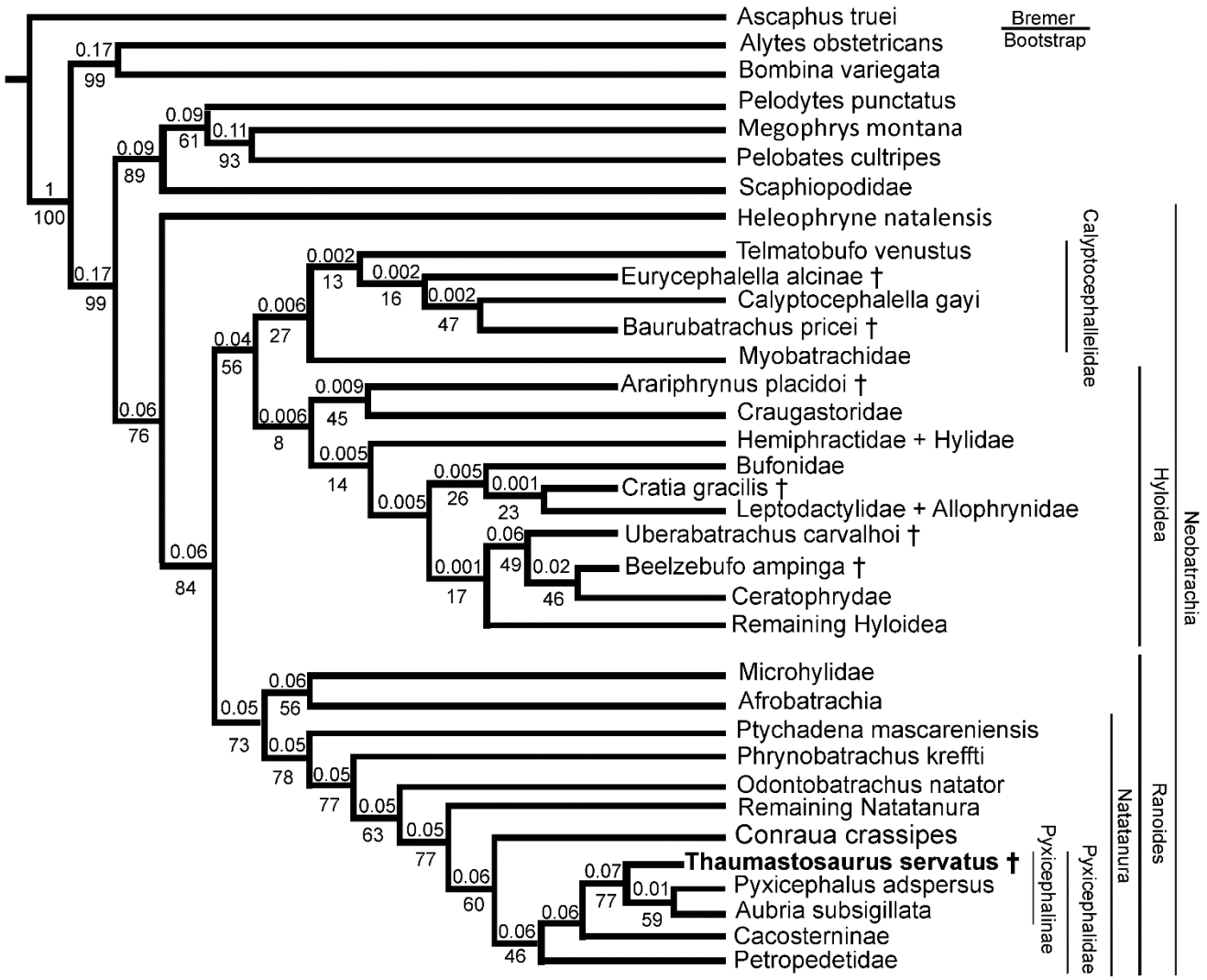
Ascaphus truei
Alytes obstetricans
Bombina variegata
Pelodytes punctatus
Megophrys montana
Pelobates cultripes
Scaphiopodidae
Heleophryne natalensis
Telmatobufo venustus
Eurycephalella alcinae †
Calyptocephalella gayi
Baurubatrachus pricei †
Myobatrachidae
Araripedidae
Craugastoridae
Hemiphractidae + Hylidae
Bufonidae
Cratia gracilis †
Leptodactylidae + Allophrynidae
Uberabatrachus carvalhoi †
Beelzebufo ampinga †
Ceratophrydae
Remaining Hyloidea
Microhylidae
Afrobatrachia
Ptychadena mascareniensis
Phrynobatrachus krefftii
Odontobatrachus natator
Remaining Natatanura
Conraua crassipes
Thaumastosaurus servatus †
Pyxicephalus adspersus
Aubria subsigillata
Cacosterninae
Petropedetidae
Bremer
Bootstrap
Calyptocephallelidae
Hyloidea
Neobatrachia
Ranoides
Natatanura
Pyxicephalidae
Pyxicephalinae